J. Fluid Mech. (2020), *vol.* 893, A17. © The Author(s), 2020.
Published by Cambridge University Press
doi:10.1017/jfm.2020.226

Evolution of a vortex in a strongly stratified shear flow. Part 1. Asymptotic analysis

Julien Bonnici[1] **and Paul Billant**[1,†]

[1]LadHyX, CNRS, École Polytechnique, 91128 Palaiseau CEDEX, France

(Received 20 July 2019; revised 28 January 2020; accepted 17 March 2020)

In this paper, we investigate the dynamics of an initially vertical vortex embedded in a shear flow in a stratified fluid by means of a long-wavelength analysis. The main goal is to determine, whether or not, the Kelvin–Helmholtz instability can develop unconditionally as speculated by Lilly (*J. Atmos. Sci.*, vol. 40, 1983, pp. 749–761). The analysis is performed in the case of the Lamb–Oseen vortex profile and a shear flow uniform in the horizontal and varying sinusoidally along the vertical using the assumption $\hat{k}_z a_0 F_h \ll 1$, where $\hat{k}_z$ is the vertical wavenumber, a_0 the vortex radius and F_h the horizontal Froude number based on the circulation of the vortex. The results show that the vortex axis is advected not only in the direction of the shear flow but also in the perpendicular direction owing to the self-induced motion of the vortex. In addition, internal waves are transiently excited at the beginning, generating an initial non-hydrostatic regime. Their relative effects on the displacements of the vortex axis are weak except initially. The angular velocity of the vortex decays owing to a dynamic effect and viscous effects related to the vertical shear. The former effect is due to the squeezing of isopycnals in the vortex core, which implies a decrease of the vertical vorticity to satisfy potential vorticity conservation. In addition, a horizontal velocity field with an azimuthal wavenumber $m = 2$ is generated, meaning that the shape of the vortex becomes slightly elliptical. We further show that the minimum asymptotic Richardson number is bounded, $\min(Ri) > 3.43$, when $\hat{k}_z a_0 F_h \ll 1$ and therefore cannot go below the critical value $1/4$. This is because the growth of the vertical shear of the horizontal velocity of the vortex saturates owing to the decay of its angular velocity and because the squeezing of isopycnals increases the stratification strength. This suggests that the shear instability cannot always develop in strongly stratified flows, contrary to the conjecture of Lilly (as above). These predictions will be tested against direct numerical simulations in Part 2.

Key words: vortex dynamics, stratified flows, transition to turbulence

1. Introduction

Stratified turbulence is strongly anisotropic with predominantly horizontal motions but high shear along the vertical (Riley & Lelong 2000). Such layered structure

† Email address for correspondence: billant@ladhyx.polytechnique.fr

https://doi.org/10.1017/jfm.2020.226 Published online by Cambridge University Press

inherently promotes the shear instability, which breaks down the layers into smaller-scale turbulence (Lilly 1983; Riley & deBruynKops 2003; Lindborg 2006). This is thought to be one of the main mechanisms that accomplish the direct energy cascade towards small scales in stratified turbulence (Laval, McWilliams & Dubrulle 2003; Riley & deBruynKops 2003; Brethouwer *et al.* 2007; Deloncle, Billant & Chomaz 2008; Augier & Billant 2011; Augier, Chomaz & Billant 2012; Waite 2013).

In his pioneering paper on strongly stratified flows, Lilly (1983) conjectured a simple mechanism for the growth of the vertical shear. He considered a uniform horizontal flow directed along a given direction, let us say x, and vertically sheared: $\boldsymbol{U} = U(z)\boldsymbol{e}_x$ where z is the vertical coordinate. If a coherent structure with initial horizontal velocity $\boldsymbol{u}_{h0}(x, y, z)$ is embedded within this shear flow, it will be advected differentially depending on the vertical position:

$$\frac{\partial \boldsymbol{u}_h}{\partial t} = -U\frac{\partial \boldsymbol{u}_h}{\partial x}. \tag{1.1}$$

Lilly further assumed that the coupling along the vertical is weak in the limit of strong stratification. When the vertical coupling is zero, the flow consists of a stack of horizontal two-dimensional flows evolving independently at each level z. Then, the solution at any time is simply $\boldsymbol{u}_h(x, y, z, t) = \boldsymbol{u}_{h0}(x - U(z)t, y, z)$. This shows that the vertical shear should grow algebraically with time according to

$$\frac{\partial \boldsymbol{u}_h}{\partial z} = -\frac{\mathrm{d}U}{\mathrm{d}z}t\frac{\partial \boldsymbol{u}_{h0}}{\partial x} + \frac{\partial \boldsymbol{u}_{h0}}{\partial z}. \tag{1.2}$$

On this basis, Lilly (1983) argued that the Richardson number should sooner or later reach the critical value $1/4$ for the onset of the shear instability (Howard 1961; Miles 1961). However, a key assumption behind this conjecture is that there is no vertical coupling. This derives directly from Lilly's assumption that the vertical Froude number tends to zero in the limit of strong stratification. It is now acknowledged that the vertical Froude number remains of order unity because the typical vertical length scale is the buoyancy length scale in strongly stratified flows (see, among others, Herring & Métais (1989), Billant & Chomaz (2000, 2001), Godeferd & Staquet (2003), Laval *et al.* (2003), Waite & Bartello (2004), Lindborg (2006)).

It is therefore unknown whether or not this mechanism for the growth of the vertical shear is valid. In order to answer this question, we have considered the particular case of an initially vertical vortex in an ambient vertically sheared flow in a stratified fluid. This flow configuration is sketched in figure 1 together with the example of a direct numerical simulation illustrating the vortex evolution. In the present paper, we shall study the dynamics of this flow by an asymptotic analysis while direct numerical simulations will be performed in Part 2 (Billant & Bonnici 2020).

The dynamics of an isolated vortex in an ambient sheared flow has been studied before in stratified rotating fluids in order to understand the dynamics of atmospheric tropical cyclones (Jones 1995, 2000*a*,*b*, 2004; Sutyrin & Morel 1997; Frank & Ritchie 1999; Reasor, Montgomery & Grasso 2004; Päschke *et al.* 2012) or oceanic vortices (Vandermeirsch, Morel & Sutyrin 2001, 2002). In particular, Jones (1995), using a three-dimensional continuous hydrostatic primitive equation model, has shown that an initially barotropic vortex in a linear shear flow tilts in the shear direction but also executes a cyclonic rotation about its mid-level centre. Päschke *et al.* (2012) have derived asymptotic equations for the motion of the vortex centre in the case of a weak shear flow.

https://doi.org/10.1017/jfm.2020.226 Published online by Cambridge University Press

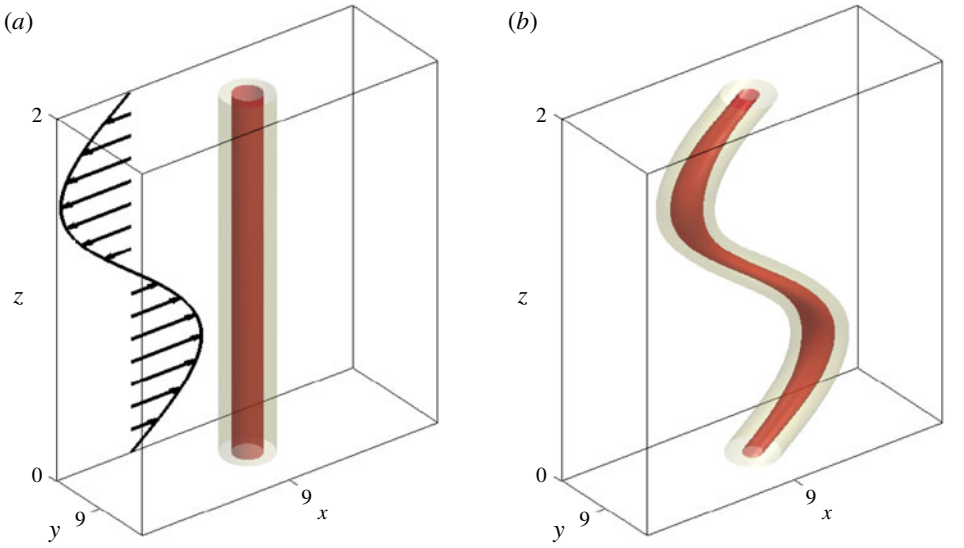


FIGURE 1. (*a*) Sketch of the flow configuration studied in this paper. The ambient shear flow $U(z)\boldsymbol{e}_x$ is represented by the black vectors. The dark grey (red) and light grey (yellow) contours show two levels of the potential vorticity of the vortex at $t = 0$. (*b*) Potential vorticity contours at $t = 20$ obtained from a direct numerical simulation for the Froude and Reynolds numbers $F_h = 0.1$, $Re = 6000$ and the shear flow $U = U_S \sin(k_z z)$ with $U_S = 0.2$ and $k_z = \pi$. These parameters are defined in § 2. See Billant & Bonnici (2020) for the details of the numerical simulations.

The influence of a vertical shear on an initially aligned vortex has also been investigated by means of quasi-geostrophic two-layer models (Marshall & Parthasarathy 1993; DeMaria 1996; Smith, Ulrich & Sneddon 2000; Vandermeirsch *et al.* 2001, 2002). Marshall & Parthasarathy (1993) have reported two distinct evolutions depending on the strength of the vortices compared to the shear. When the advection by the shear is below a critical value, the vortices in each layer are offset and rotate about each other. Conversely, when the advection is sufficiently strong, the two vortices are continuously advected away from each other. These two regimes have been called non-tearing and tearing regimes, respectively.

In contrast, the dynamics of an isolated vortex subjected to a vertical shear in stratified non-rotating fluids has been little investigated so far. Boulanger, Meunier & Le Dizès (2007, 2008) have considered the dynamics of a vortex slightly tilted with respect to the direction of stratification. However, the tilt of the vortex is not created by an external shear flow but by the method of generation of the vortex. Majda & Grote (1997) have studied the effect of a vertically sheared mean horizontal flow on a vortex pair but only by means of the reduced equations of Lilly (1983), which are valid in the limits of zero vertical and horizontal Froude numbers. Here and in Part 2 (Billant & Bonnici 2020), we will study the dynamics of a Lamb–Oseen vortex in a sinusoidally sheared flow using the full Navier–Stokes equations under the Boussinesq approximation with the aim of testing Lilly's conjecture for the growth of vertical shear.

In the present paper, an asymptotic analysis is conducted in § 3 for long vertical wavelength following a similar approach to that used by Billant (2010) to describe the zigzag instability of columnar vortices in stratified rotating fluids. This analysis

https://doi.org/10.1017/jfm.2020.226 Published online by Cambridge University Press

provides the governing equations for the displacements of the vortex centre (§ 3.2.1) and the evolution of its vertical vorticity (§ 3.2.2) due to the shear flow. These equations are further analysed in §§ 4.2 and 4.1, respectively. The evolution of the Richardson number is then studied in § 4.3. These asymptotic predictions will be compared to direct numerical simulations (DNS) in Part 2.

2. Formulation of the problem

2.1. *Governing equations*

We consider the incompressible Navier–Stokes equations written within the Boussinesq approximation:

$$\boldsymbol{\nabla}\cdot\boldsymbol{u}=0, \tag{2.1}$$

$$\frac{\partial \boldsymbol{u}}{\partial t}+(\boldsymbol{u}\cdot\boldsymbol{\nabla})\boldsymbol{u}=-\boldsymbol{\nabla}\left(\frac{p}{\rho_0}\right)+b\boldsymbol{e}_z+\nu\nabla^2\boldsymbol{u}, \tag{2.2}$$

$$\frac{\partial b}{\partial t}+\boldsymbol{u}\cdot\boldsymbol{\nabla}b+N^2w=\kappa\nabla^2 b. \tag{2.3}$$

Here $\boldsymbol{u}=(u,v,w)$ is the velocity field in Cartesian coordinates (x,y,z), p the pressure, $b=-g\rho/\rho_0$ the buoyancy, g the gravity, $\boldsymbol{e}_z$ the vertical unit vector oriented upwards, ν the viscosity and κ the buoyancy diffusivity. The total density field ρ_t has been decomposed as $\rho_t(\boldsymbol{x},t)=\rho_0+\bar{\rho}(z)+\rho(\boldsymbol{x},t)$, ρ_0 being a constant reference density, $\bar{\rho}$ a linear mean density profile varying with the vertical coordinate z and $\rho(\boldsymbol{x},t)$ a perturbation density. The Brunt–Väisälä frequency measuring the ambient stratification $N=\sqrt{-(g/\rho_0)\,\mathrm{d}\bar{\rho}/\mathrm{d}z}$ is assumed constant.

2.2. *Initial condition*

The initial flow is made of a columnar vortex embedded in a sinusoidal shear flow of the form $\boldsymbol{U}_S=U(z)\boldsymbol{e}_x$, where $U(z)=\hat{U}_S\sin(\hat{k}_z z)$, $\boldsymbol{e}_x$ is the unit vector in the x direction, $\hat{U}_S$ the amplitude and $\hat{k}_z$ the vertical wavenumber. The vortex is chosen to have a Lamb–Oseen profile,

$$\boldsymbol{u}_v=\frac{\Gamma}{2\pi r}\left[1-\exp\left(-\frac{r^2}{a_0^2}\right)\right]\boldsymbol{e}_\theta, \tag{2.4}$$

where (r,θ,z) are cylindrical coordinates such that $x=r\cos(\theta)$ and $y=r\sin(\theta)$, Γ is the vortex circulation, a_0 its radius and $\boldsymbol{e}_\theta$ the unit vector in the azimuthal direction. Without loss of generality, the vortex circulation will be considered positive in the following.

The total initial flow is therefore

$$\boldsymbol{u}(\boldsymbol{x},t=0)=\boldsymbol{U}_S+\boldsymbol{u}_v. \tag{2.5}$$

2.3. *Non-dimensionalization*

Equations (2.1)–(2.3) are non-dimensionalized by the characteristics of the vortex: the length and time units are taken as the vortex radius a_0 and the turnover time scale $2\pi a_0^2/\Gamma$. Keeping the same notation for the non-dimensional variables, the dimensionless equations read

$$\boldsymbol{\nabla}_h\cdot\boldsymbol{u}_h+\frac{\partial w}{\partial z}=0, \tag{2.6}$$

https://doi.org/10.1017/jfm.2020.226 Published online by Cambridge University Press

$$\frac{\partial \boldsymbol{u}_h}{\partial t} + (\boldsymbol{u}_h \cdot \boldsymbol{\nabla}_h)\,\boldsymbol{u}_h + w\frac{\partial \boldsymbol{u}_h}{\partial z} = -\boldsymbol{\nabla}_h p + \frac{1}{Re}\nabla^2 \boldsymbol{u}_h, \tag{2.7}$$

$$\frac{\partial w}{\partial t} + \boldsymbol{u}_h \cdot \boldsymbol{\nabla}_h w + w\frac{\partial w}{\partial z} = -\frac{\partial p}{\partial z} + b + \frac{1}{Re}\nabla^2 w, \tag{2.8}$$

$$\frac{\partial b}{\partial t} + \boldsymbol{u}_h \cdot \boldsymbol{\nabla}_h b + w\frac{\partial b}{\partial z} = -\frac{w}{F_h^2} + \frac{1}{ReSc}\nabla^2 b, \tag{2.9}$$

where $\boldsymbol{u}_h$ denotes the horizontal velocity. The Reynolds and Froude numbers are defined as

$$Re = \frac{\Gamma}{2\pi\nu}, \quad F_h = \frac{\Gamma}{2\pi a_0^2 N}, \tag{2.10a,b}$$

and $Sc = \nu/\kappa$ is the Schmidt number.

In non-dimensional form, the velocities of the shear flow and the vortex become

$$\boldsymbol{U}_S = U_S \sin(k_z z)\boldsymbol{e}_x, \quad \boldsymbol{u}_v = u_\theta(r)\boldsymbol{e}_\theta = \frac{1-\exp(-r^2)}{r}\boldsymbol{e}_\theta, \tag{2.11a,b}$$

where $U_S = \hat{U}_S 2\pi a_0/\Gamma$ and $k_z = \hat{k}_z a_0$. The corresponding wavelength is $l_z = 2\pi/k_z$.

3. Long-wavelength dynamics of the vortex

The dynamics of the vortex can be described asymptotically for finite time in the limit of small vertical wavenumber. Indeed, when $k_z = 0$, i.e. in the two-dimensional limit, an exact solution is

$$\boldsymbol{u}_h = \boldsymbol{u}_{h0}(x - Ut, y) + U\boldsymbol{e}_x, \tag{3.1}$$

which means that the vortex is simply advected at constant speed U. This solution is expected to remain valid at leading order when $\varepsilon = k_z F_h$ is small, i.e. when the vertical variations $\partial/\partial z$ of $U(z)$ rescaled by the Froude number F_h are weak:

$$\varepsilon = O\left(F_h \frac{\partial}{\partial z}\right) \ll 1. \tag{3.2}$$

We consider that the small parameter is $k_z F_h$ instead of k_z because of the self-similarity of strongly stratified fluids (Billant & Chomaz 2001). Indeed, this self-similarity implies that the horizontal velocity depends on F_h and k_z only through their product $k_z F_h$ when the fluid is strongly stratified, $F_h < 1$. This means that the condition $\varepsilon \ll 1$ can be fulfilled either by having $k_z \ll 1$, $F_h < 1$ or $k_z \gg 1$, $F_h \ll 1$ provided that $k_z F_h \ll 1$. In order to encompass both cases, the first part of the asymptotic analysis will only assume $F_h < 1$. Nevertheless, the second part will assume $F_h \ll 1$ in order to simplify the calculations. Consistently with (3.2), we rescale the vertical coordinate as

$$\tilde{z} = \frac{\varepsilon}{F_h} z, \tag{3.3}$$

so that $\partial/\partial\tilde{z} = O(1)$ and the rescaled wavenumber is $\tilde{k}_z = k_z F_h/\varepsilon \equiv 1$. Then, we can express the horizontal velocity in the form of an asymptotic expansion:

$$\boldsymbol{u}_h = \boldsymbol{u}_{h0}(x - U(\tilde{z})t - \delta x, y - \delta y, \tilde{z}, \tau) + U(\tilde{z})\boldsymbol{e}_x + \varepsilon^2 \boldsymbol{u}_{h1}(x, y, \tilde{z}, t, \tau) + O(\varepsilon^4), \tag{3.4}$$

https://doi.org/10.1017/jfm.2020.226 Published online by Cambridge University Press

where $\delta x(\tilde{z},\tau)$ and $\delta y(\tilde{z},\tau)$ are corrections to the displacements of the vortex centre varying along the vertical and with the slow time scale $\tau=\varepsilon^2 t$. This choice for the scaling of the slow time scale is explained in detail in appendix A. We also define local horizontal Cartesian coordinates $(\tilde{x},\tilde{y})$ centred on the vortex centre at the level $\tilde{z}$:

$$\tilde{x}=x-U(\tilde{z})t-\delta x(\tilde{z},\tau),\quad \tilde{y}=y-\delta y(\tilde{z},\tau). \tag{3.5a,b}$$

The cylindrical coordinates associated with these new coordinates are denoted with a tilde, $(\tilde{x},\tilde{y})=(\tilde{r}\cos\tilde{\theta},\tilde{r}\sin\tilde{\theta})$. In addition to the horizontal velocity, the other fields are expanded in the form

$$p=p_0(\tilde{x},\tilde{y},\tau)+\varepsilon^2 p_1(\tilde{x},\tilde{y},\tilde{z},t,\tau)+O(\varepsilon^4), \tag{3.6}$$

$$w=\varepsilon F_h[w_0(\tilde{x},\tilde{y},\tilde{z},t,\tau)+\varepsilon^2 w_1(\tilde{x},\tilde{y},\tilde{z},t,\tau)+O(\varepsilon^4)], \tag{3.7}$$

$$b=\frac{\varepsilon}{F_h}[b_0(\tilde{x},\tilde{y},\tilde{z},t,\tau)+\varepsilon^2 b_1(\tilde{x},\tilde{y},\tilde{z},t,\tau)+O(\varepsilon^4)], \tag{3.8}$$

where the vertical velocity and the buoyancy have been scaled by εF_h and ε/F_h, respectively, for convenience. These scalings are equivalent to those of Billant & Chomaz (2001) for strongly stratified flows. Weak viscous effects will also be taken into account by assuming a large buoyancy Reynolds number such that

$$\frac{1}{Re\,F_h^2}=\frac{\varepsilon^2}{\tilde{Re}_b}, \tag{3.9}$$

where $\tilde{Re}_b=O(1)$.

The expansions (3.4), (3.6), (3.7) and (3.8) will be introduced in the governing equations (2.6)–(2.9). It will be useful to consider also the equation for the vertical vorticity $\zeta=\partial v/\partial x-\partial u/\partial y$:

$$\frac{\partial\zeta}{\partial t}+\boldsymbol{u}_h\cdot\boldsymbol{\nabla}_h\zeta+w\frac{\partial\zeta}{\partial z}=\boldsymbol{\omega}_h\cdot\boldsymbol{\nabla}_h w+\zeta\frac{\partial w}{\partial z}+\frac{1}{Re}\nabla^2\zeta, \tag{3.10}$$

where $\boldsymbol{\omega}_h$ is the horizontal vorticity.

Because of the introduction of the local coordinates $(\tilde{x},\tilde{y})$ that depend on t, τ and $\tilde{z}$ (see (3.5)), the time and vertical derivatives of any quantity Λ in (2.6)–(2.9) and (3.10) become

$$\frac{\partial\Lambda}{\partial t}=\left(\frac{\partial\Lambda}{\partial t}\right)_{\tilde{x},\tilde{y},\tau}-U(\tilde{z})\frac{\partial\Lambda}{\partial\tilde{x}}+\varepsilon^2\left[\left(\frac{\partial\Lambda}{\partial\tau}\right)_{\tilde{x},\tilde{y},t}-\frac{\partial\delta x}{\partial\tau}\frac{\partial\Lambda}{\partial\tilde{x}}-\frac{\partial\delta y}{\partial\tau}\frac{\partial\Lambda}{\partial\tilde{y}}\right], \tag{3.11}$$

$$\frac{\partial\Lambda}{\partial z}=\frac{\varepsilon}{F_h}\left[\left(\frac{\partial\Lambda}{\partial\tilde{z}}\right)_{\tilde{x},\tilde{y}}-\left(t\frac{\mathrm{d}U}{\mathrm{d}\tilde{z}}+\frac{\partial\delta x}{\partial\tilde{z}}\right)\frac{\partial\Lambda}{\partial\tilde{x}}-\frac{\partial\delta y}{\partial\tilde{z}}\frac{\partial\Lambda}{\partial\tilde{y}}\right]. \tag{3.12}$$

It is important to remark on the presence of the term $t\,\mathrm{d}U/\mathrm{d}\tilde{z}$ in (3.12). Because of this term, the long-wavelength assumption (3.2) is *a priori* expected to be no longer valid when $\varepsilon t\,\mathrm{d}U/\mathrm{d}\tilde{z}>1$, i.e. when $\varepsilon t>1$, since the shear flow $U=U_S\sin(\tilde{k}_z\tilde{z})$ will be considered of order unity in the following.

Although the present asymptotic analysis is strictly valid only when $t\ll 1/\varepsilon$, we should keep in mind that the time scale $\tilde{\tau}=\varepsilon t=O(1)$ is of particular interest even if

https://doi.org/10.1017/jfm.2020.226 Published online by Cambridge University Press

a rigorous asymptotic analysis cannot be conducted under this assumption. For this reason, we will also keep the leading-order viscous effects that are of order unity when $t = O(1/\varepsilon)$, i.e. $\tilde{\tau} = O(1)$. The purpose is to be as general as possible.

We now solve the leading-order problem in § 3.1 and the first-order problem in § 3.2. The reader interested only in the resulting equations can jump directly to §§ 4.1 and 4.2 where the equations for the angular velocity of the vortex and the displacements $(\delta x, \delta y)$ are analysed, respectively.

3.1. *Leading-order problem*

At leading order, (2.6)–(2.9) reduce to

$$\boldsymbol{\nabla}_h \cdot \boldsymbol{u}_{h0} = 0, \tag{3.13}$$

$$(\boldsymbol{u}_{h0} \cdot \boldsymbol{\nabla}_h)\, \boldsymbol{u}_{h0} = -\boldsymbol{\nabla}_h p_0, \tag{3.14}$$

$$F_h^2 \left[\left(\frac{\partial w_0}{\partial t} \right)_{\tilde{x},\tilde{y},\tau} + \boldsymbol{u}_{h0} \cdot \boldsymbol{\nabla}_h w_0 \right] = -\frac{\partial p_0}{\partial \tilde{z}} + b_0, \tag{3.15}$$

$$\left(\frac{\partial b_0}{\partial t} \right)_{\tilde{x},\tilde{y},\tau} + \boldsymbol{u}_{h0} \cdot \boldsymbol{\nabla}_h b_0 = -w_0, \tag{3.16}$$

where the operator $\boldsymbol{\nabla}_h$ is with respect to $\tilde{x}$ and $\tilde{y}$, or equivalently $\tilde{r}$ and $\tilde{\theta}$. Note that the advection by the shear flow $U(\tilde{z})\, \partial/\partial \tilde{x}$ is absent in (3.14)–(3.16) since it cancels with the term coming from the time derivative (see (3.11)).

Equations (3.13)–(3.14) are the steady two-dimensional Euler equations. Consistently with the initial conditions chosen in §2.2, we take an axisymmetric vortex at leading order, namely $\boldsymbol{u}_{h0} = \tilde{r}\Omega(\tilde{r}, \tilde{z}, \tau)\boldsymbol{e}_{\tilde{\theta}}$. Even if the angular velocity does not depend on the vertical coordinate $\tilde{z}$ initially, we will see that such dependence appears with time. In order to simplify the notation, Ω is not denoted with a subscript 0 although it is a zeroth-order quantity. Then, equation (3.14) reduces to

$$\frac{\partial p_0}{\partial \tilde{r}} = \tilde{r}\Omega^2, \tag{3.17}$$

which is the balance between the centrifugal force and the radial pressure gradient as if the shear flow were absent. This gives

$$p_0 = \int^{\tilde{r}} \xi\, \Omega^2(\xi, \tilde{z}, \tau)\, \mathrm{d}\xi. \tag{3.18}$$

Therefore, the vertical pressure gradient is given by

$$\frac{\partial p_0}{\partial \tilde{z}} = \left(\frac{\partial p_0}{\partial \tilde{z}} \right)_{\tilde{r},\tilde{\theta}} + \frac{\partial \tilde{r}}{\partial \tilde{z}} \frac{\partial p_0}{\partial \tilde{r}} + \frac{\partial \tilde{\theta}}{\partial \tilde{z}} \frac{\partial p_0}{\partial \tilde{\theta}} \tag{3.19}$$

$$= \int^{\tilde{r}} \xi \frac{\partial \Omega^2}{\partial \tilde{z}}\, \mathrm{d}\xi - \left[\cos(\tilde{\theta}) \left(\frac{\mathrm{d}U}{\mathrm{d}\tilde{z}} t + \frac{\partial \delta x}{\partial \tilde{z}} \right) + \sin(\tilde{\theta}) \frac{\partial \delta y}{\partial \tilde{z}} \right] \tilde{r}\Omega^2, \tag{3.20}$$

since (3.5) implies

$$\frac{\partial \tilde{r}}{\partial \tilde{z}} = -\cos(\tilde{\theta}) \left(\frac{\mathrm{d}U}{\mathrm{d}\tilde{z}} t + \frac{\partial \delta x}{\partial \tilde{z}} \right) - \sin(\tilde{\theta}) \frac{\partial \delta y}{\partial \tilde{z}}, \tag{3.21}$$

https://doi.org/10.1017/jfm.2020.226 Published online by Cambridge University Press

$$\frac{\partial\tilde{\theta}}{\partial\tilde{z}} = \frac{\sin(\tilde{\theta})}{\tilde{r}}\left(\frac{\mathrm{d}U}{\mathrm{d}\tilde{z}}t + \frac{\partial\delta x}{\partial\tilde{z}}\right) - \frac{\cos(\tilde{\theta})}{\tilde{r}}\frac{\partial\delta y}{\partial\tilde{z}}. \tag{3.22}$$

Equation (3.20) shows that a vertical pressure gradient appears as soon as the vortex axis is inclined by the ambient shear (second term on the right-hand side) and if the angular velocity Ω varies with $\tilde{z}$ (first term). This vertical pressure gradient will force a vertical velocity field and a buoyancy field through (3.15) and (3.16). Since the fluid is strongly stratified, most of the vertical pressure gradient is balanced by buoyancy (i.e. the hydrostatic balance) whereas a vertical velocity is generated mainly to satisfy the buoyancy equation. Using (3.20) and the expression for $\boldsymbol{u}_{h0}$, they can be found as

$$\begin{aligned} w_0 \;=\; & \mathscr{C}\frac{\mathrm{d}U}{\mathrm{d}\tilde{z}}\left[\cos(\tilde{\theta})\mathscr{F} - t\sin(\tilde{\theta})\Omega - \mathscr{F}\cos(\Omega t-\tilde{\theta})\cos\left(\frac{t}{F_h}\right)\right. \\ & \left. -\; 2\mathscr{G}\sin(\Omega t-\tilde{\theta})\sin\left(\frac{t}{F_h}\right)\right] + \left[-\sin(\tilde{\theta})\frac{\partial\delta x}{\partial\tilde{z}} + \cos(\tilde{\theta})\frac{\partial\delta y}{\partial\tilde{z}}\right]\mathscr{C}\Omega, \end{aligned} \tag{3.23}$$

$$\begin{aligned} b_0 \;=\; & -F_h\mathscr{C}\frac{\mathrm{d}U}{\mathrm{d}\tilde{z}}\left[2\sin(\tilde{\theta})\mathscr{G} + \frac{t}{F_h}\cos(\tilde{\theta}) + 2\mathscr{G}\sin(\Omega t-\tilde{\theta})\cos\left(\frac{t}{F_h}\right)\right. \\ & \left. -\;\mathscr{F}\cos(\Omega t-\tilde{\theta})\sin\left(\frac{t}{F_h}\right)\right] - \left[\cos(\tilde{\theta})\frac{\partial\delta x}{\partial\tilde{z}} + \sin(\tilde{\theta})\frac{\partial\delta y}{\partial\tilde{z}}\right]\mathscr{C} \\ & +\int^{\tilde{r}}\xi\frac{\partial\Omega^2}{\partial\tilde{z}}\,\mathrm{d}\xi, \end{aligned} \tag{3.24}$$

where the functions

$$\mathscr{C} = \frac{\tilde{r}\Omega^2}{1-F_h^2\Omega^2}, \quad \mathscr{F} = \frac{1+F_h^2\Omega^2}{1-F_h^2\Omega^2}, \quad \mathscr{G} = \frac{F_h\Omega}{1-F_h^2\Omega^2} \tag{3.25a–c}$$

have no singular point since $\Omega < 1/F_h$ for all radii when $F_h < 1$. We have imposed that the vertical velocity and the buoyancy are null at $t = \tau = 0$ since the vortex is strictly vertical and uniform at the start-up of the evolution.

The vertical velocity and buoyancy equations (3.23) and (3.24) contain four types of terms evolving on three different time scales:

(i) The first two terms on the right-hand sides grow linearly with the fast time t in response to the shear flow $U(\tilde{z})$.

(ii) Internal waves (third and fourth terms) oscillating at the frequency $1/F_h$ (i.e. the Brunt–Väisälä frequency in dimensional units) are generated at the onset of the motion. Strictly speaking, the coefficients in front of these terms are fixed at $\tau = 0$. However, it is also legitimate to let these terms evolve on τ like the other terms since the evolution over the slow time scale τ is a higher-order effect.

(iii) The fifth and sixth terms are due to the slow evolution of the displacement corrections δx and δy.

(iv) A buoyancy perturbation (last term of (3.24)) which is generated by the vertical variation of the angular velocity through the hydrostatic balance.

In the limit $t \ll 1$, $\tau \ll 1$, (3.23) and (3.24) rescaled by εF_h and ε/F_h become at leading order

$$w = \varepsilon F_h w_0 = \frac{1}{2}\cos(\tilde{\theta})\tilde{r}\Omega^2\frac{\mathrm{d}U}{\mathrm{d}z}t^2 + O(t^3,\tau), \tag{3.26}$$

https://doi.org/10.1017/jfm.2020.226 Published online by Cambridge University Press

$$b = \varepsilon \frac{b_0}{F_h} = -\frac{1}{6F_h^2} \cos(\tilde{\theta}) \tilde{r} \Omega^2 \frac{\mathrm{d}U}{\mathrm{d}z} t^3 + O(t^4, \tau), \tag{3.27}$$

since δx, δy and the vertical variations of Ω are negligible for $\tau \ll 1$. The vertical velocity and buoyancy are therefore of the form $w \propto t^2$ and $b \propto t^3$ at leading order in time. By means of an asymptotic expansion for small times, it can be shown that these scaling laws are in fact valid for any finite vertical wavenumber (Bonnici 2018). Equations (3.26) and (3.27) imply that the ratio of the vertical acceleration to the buoyancy is

$$\left| \frac{1}{b} \frac{\mathrm{D}w}{\mathrm{D}t} \right| = 6 \left(\frac{F_h}{t} \right)^2. \tag{3.28}$$

Therefore, for small times such that $t \ll F_h$, the buoyancy is negligible relative to the vertical acceleration, meaning that the dynamics is initially non-hydrostatic. This comes from the generation of internal waves of frequency $1/F_h$. This transient non-hydrostatic phase lasts until $t = O(F_h)$. For $t \gg F_h$, the amplitude of the waves in (3.23) and (3.24) will become small relative to the terms that grow linearly with time so that $w \propto F_h^2 t$ and $b \propto t$. The hydrostatic balance will therefore be recovered since $w/b = O(F_h^2)$.

Although the components of the internal waves have been determined explicitly in (3.23) and (3.24), it should be stressed that their asymptotic calculation is actually not uniformly valid when $\varepsilon = k_z F_h$ is small. It is valid only when k_z is small but not if F_h is small and k_z finite. This limitation comes from the fact that internal waves oscillating at the fast frequency $1/F_h$ do not depend on k_z and F_h only through the self-similar parameter $k_z F_h$ unlike advective motions in strongly stratified fluids (Billant & Chomaz 2001). This can be easily seen by considering the full dispersion relation of internal waves in a medium at rest in Cartesian coordinates, $\omega = k_h/(F_h\sqrt{k_h^2 + k_z^2})$, where k_h is the horizontal wavenumber, which is assumed to be of order unity. The frequency ω tends to $1/F_h$ if $k_z \ll 1$ but not if $k_z = O(1)$ and $F_h \ll 1$. In the latter case, the internal waves could be computed only numerically. However, we have not attempted such a numerical computation because we will see in Part 2 that the waves actually quickly propagate away from the vortex core when k_z is finite. This is due to the fact that their radial group velocity, which is proportional to k_z^2/F_h, is large in this case. Thus, their effect in the vortex neighbourhood manifests only initially and is weak so that they can be completely neglected for finite k_z.

3.2. *First-order problem*

At first order, it is more convenient to consider the divergence equation and the equation for the vertical vorticity $\zeta_1 = \partial v_1/\partial \tilde{x} - \partial u_1/\partial \tilde{y}$:

$$\boldsymbol{\nabla}_h \cdot \boldsymbol{u}_{h1} = -\left[\frac{\partial w_0}{\partial \tilde{z}} + \frac{\partial \tilde{r}}{\partial \tilde{z}} \frac{\partial w_0}{\partial \tilde{r}} + \frac{\partial \tilde{\theta}}{\partial \tilde{z}} \frac{\partial w_0}{\partial \tilde{\theta}} \right], \tag{3.29}$$

$$\begin{aligned} \frac{\partial \zeta_1}{\partial t} + \boldsymbol{u}_{h0} \cdot \boldsymbol{\nabla}_h \zeta_1 + \boldsymbol{u}_{h1} \cdot \boldsymbol{\nabla}_h \zeta_0 &= -\frac{\partial \zeta_0}{\partial \tau} + \cos(\tilde{\theta}) \frac{\partial \delta x}{\partial \tau} \frac{\partial \zeta_0}{\partial \tilde{r}} + \sin(\tilde{\theta}) \frac{\partial \delta y}{\partial \tau} \frac{\partial \zeta_0}{\partial \tilde{r}} \\ &\quad + \left[\frac{\mathrm{d}U}{\mathrm{d}\tilde{z}} + \frac{\partial \tilde{r}}{\partial \tilde{z}} \frac{\partial u_0}{\partial \tilde{r}} + \frac{\partial \tilde{\theta}}{\partial \tilde{z}} \frac{\partial u_0}{\partial \tilde{\theta}} + \frac{\partial u_0}{\partial \tilde{z}} \right] \frac{\partial w_0}{\partial \tilde{y}} \end{aligned}$$

https://doi.org/10.1017/jfm.2020.226 Published online by Cambridge University Press

$$- \left[\frac{\partial \tilde{r}}{\partial \tilde{z}}\frac{\partial v_0}{\partial \tilde{r}} + \frac{\partial \tilde{\theta}}{\partial \tilde{z}}\frac{\partial v_0}{\partial \tilde{\theta}} + \frac{\partial v_0}{\partial \tilde{z}}\right]\frac{\partial w_0}{\partial \tilde{x}}$$
$$+ \zeta_0\left[\frac{\partial w_0}{\partial \tilde{z}} + \frac{\partial \tilde{r}}{\partial \tilde{z}}\frac{\partial w_0}{\partial \tilde{r}} + \frac{\partial \tilde{\theta}}{\partial \tilde{z}}\frac{\partial w_0}{\partial \tilde{\theta}}\right]$$
$$- w_0\left[\frac{\partial \tilde{r}}{\partial \tilde{z}}\frac{\partial \zeta_0}{\partial \tilde{r}} + \frac{\partial \zeta_0}{\partial \tilde{z}}\right] + \frac{F_h^2\nabla^2\zeta_0}{\tilde{Re}_b}, \tag{3.30}$$

where $\zeta_0 = 2\Omega + \tilde{r}\,\partial\Omega/\partial\tilde{r}$ is the vertical vorticity. In (3.29) and (3.30), all the time and vertical derivatives are taken at constant $(\tilde{r}, \tilde{\theta})$ but this is no longer mentioned to simplify the notation. Such convention will be always used in the following. We remind the reader also that (u_0, v_0, w_0) are the velocity components in Cartesian coordinates.

Equations (3.29) and (3.30) show that the leading-order vertical velocity w_0 forces a horizontal flow at first order. The forcing terms on the right-hand side of (3.30) correspond to the slow evolution of ζ_0 and the displacements δx, δy (first line), the tilting of horizontal vorticity into vertical vorticity (second and third lines), the stretching of vertical vorticity (fourth line), the vertical advection of vertical vorticity and viscous effects (last line). Owing to the expression of the vertical derivative (3.12) (or see (3.19)), the latter term reads

$$F_h^2\nabla^2\zeta_0 = \frac{1}{\tilde{r}}\frac{\partial}{\partial\tilde{r}}\left(\tilde{r}\frac{\partial\zeta_0}{\partial\tilde{r}}\right)\left[F_h^2 + \frac{\varepsilon^2t^2}{2}\left(\frac{\mathrm{d}U}{\mathrm{d}\tilde{z}}\right)^2\right] + \frac{\varepsilon^2t^2}{2}\tilde{r}\frac{\partial}{\partial\tilde{r}}\left(\frac{1}{\tilde{r}}\frac{\partial\zeta_0}{\partial\tilde{r}}\right)\left(\frac{\mathrm{d}U}{\mathrm{d}\tilde{z}}\right)^2\cos(2\tilde{\theta})$$
$$- \varepsilon^2t\frac{\partial\zeta_0}{\partial\tilde{r}}\frac{\mathrm{d}^2U}{\mathrm{d}\tilde{z}^2}\cos(\tilde{\theta}) - 2\varepsilon^2t\frac{\partial}{\partial\tilde{r}}\left[\frac{\partial\zeta_0}{\partial\tilde{z}}\right]\frac{\mathrm{d}U}{\mathrm{d}\tilde{z}}\cos(\tilde{\theta}) + \varepsilon^2\frac{\partial^2\zeta_0}{\partial\tilde{z}^2}, \tag{3.31}$$

where we have taken into account only the terms proportional to $t\,\mathrm{d}U/\mathrm{d}\tilde{z}$ in (3.21) and (3.22) and neglected the others. The expression (3.31) suggests that we should neglect all the terms except the first one on the right-hand side since all the others are proportional to ε^2. However, some of these terms grow like t^2 and can thus become of order unity when $\varepsilon t = O(1)$. For this reason, we will take into account in the following the first three terms (first line) which come from the horizontal and vertical dissipative terms and are of order unity or grow like $\tilde{\tau}^2 = \varepsilon^2t^2$, while the last three terms (second line) related to vertical dissipation will be neglected since they are at most of order ε for $t = O(1/\varepsilon)$. Note that, for such large time, the terms proportional to $t\,\mathrm{d}U/\mathrm{d}\tilde{z}$ in (3.21) and (3.22) are much larger than the others, justifying the approximation made to derive (3.31).

We see in (3.31) that the viscous term contains azimuthal modes $m = 0$, 1 and 2. In fact, the other forcing terms in (3.29) and (3.30) can also be decomposed into these three azimuthal modes. Looking, for example, at the divergence equation (3.29), the term $\partial w_0/\partial\tilde{z}$ will produce terms proportional to $\cos(\tilde{\theta})$ or $\sin(\tilde{\theta})$, while the other two terms will give azimuthal modes of the form $\cos(m\tilde{\theta})$ and $\sin(m\tilde{\theta})$ with $m = 0$ or $m = 2$. The right-hand side of (3.30) can be decomposed similarly into the azimuthal modes $m = 0$, 1 and 2. For this reason, (3.29) and (3.30) can be solved by decomposing the horizontal velocity into three potential and rotational components,

$$\boldsymbol{u}_{h1} = \boldsymbol{\nabla}_h(\Phi_{10} + \Phi_{11} + \Phi_{12}) - \boldsymbol{\nabla}\times(\psi_{10} + \psi_{11} + \psi_{12})\boldsymbol{e}_z, \tag{3.32}$$

https://doi.org/10.1017/jfm.2020.226 Published online by Cambridge University Press

corresponding to the azimuthal modes $m = \{0, 1, 2\}$, respectively. Then, (3.29) and (3.30) each separate into three independent equations

$$\nabla_h^2 \Phi_{1m} = \delta D_m, \tag{3.33}$$

$$\mathrm{L}(\psi_{1m}) \equiv \left[\frac{\partial}{\partial t} + \Omega \frac{\partial}{\partial \tilde{\theta}}\right] \nabla_h^2 \psi_{1m} - \frac{1}{\tilde{r}} \frac{\partial \zeta_0}{\partial \tilde{r}} \frac{\partial \psi_{1m}}{\partial \tilde{\theta}} = \delta Z_m - \frac{\partial \Phi_{1m}}{\partial \tilde{r}} \frac{\partial \zeta_0}{\partial \tilde{r}}, \tag{3.34}$$

for $m = \{0, 1, 2\}$, where $(\delta D_m, \delta Z_m)$ correspond to the terms on the right-hand side of (3.29) and (3.30) with azimuthal mode m. We will begin by solving the potential and streamfunction (Φ_{11}, ψ_{11}), which will provide the governing equations for the displacements $(\delta x, \delta y)$. The potential and streamfunction (Φ_{10}, ψ_{10}) will be determined next in § 3.2.2 and will yield an evolution equation for the angular velocity Ω, whereas (Φ_{12}, ψ_{12}) are solved in appendix D.

3.2.1. *Determination of* Φ_{11} *and* ψ_{11}

We remind the reader that the angular velocity of the vortex is assumed to vary over τ and $\tilde{z}$. However, these dependences are unknown at this stage since they will be determined only in § 3.2.2. Equation (3.33) for the potential Φ_{11} is

$$\nabla_h^2 \Phi_{11} = -\frac{\partial w_0}{\partial \tilde{z}}. \tag{3.35}$$

By imposing that Φ_{11} is not singular at $\tilde{r} = 0$ and vanishes as $\tilde{r}$ tends to infinity, the solution can be found by the method of variation of parameters as

$$\begin{aligned} \Phi_{11} \;=\; & \frac{1}{2}\left[\sin(\tilde{\theta}) \frac{\partial^2 \delta x}{\partial \tilde{z}^2} - \cos(\tilde{\theta}) \frac{\partial^2 \delta y}{\partial \tilde{z}^2}\right] \Phi_s + \frac{1}{2} t \sin(\tilde{\theta}) \Phi_{p\Omega} \frac{\mathrm{d}U}{\mathrm{d}\tilde{z}} \\ & + \frac{1}{2}\left[-\cos(\tilde{\theta}) \Phi_{pc} + t \sin(\tilde{\theta}) \Phi_{ps}\right] \frac{\mathrm{d}^2 U}{\mathrm{d}\tilde{z}^2} \\ & - \left[\Phi_{wc} \cos(\tilde{\theta}) + \Phi_{ws} \sin(\tilde{\theta})\right] \frac{\mathrm{d}^2 U}{\mathrm{d}\tilde{z}^2}, \end{aligned} \tag{3.36}$$

where Φ_s, $\Phi_{p\Omega}$, Φ_{ps}, Φ_{pc}, Φ_{wc} and Φ_{ws} are defined in appendix B. The terms associated with these potentials correspond, respectively, to the effects of the displacements (Φ_s), the vertical variations of the angular velocity $(\Phi_{p\Omega})$, the shear flow (Φ_{ps}, Φ_{pc}) and the internal waves (Φ_{wc}, Φ_{ws}). The vertical derivative of the angular velocity has been taken into account only in the leading-order term of the vertical velocity when t is large in order to compute the second term in the first line of (3.36). Indeed, since the vertical variations of Ω are significant only when t is large, at that time the vertical velocity (3.23) can be approximated by $w_0 \simeq -t \sin(\tilde{\theta}) \Omega \mathscr{C} \, \mathrm{d}U/\mathrm{d}\tilde{z}$.

Equation (3.34) for the streamfunction ψ_{11} is

$$\begin{aligned} \mathrm{L}(\psi_{11}) \;=\; & \left[\cos(\tilde{\theta}) \frac{\partial \delta x}{\partial \tau} + \sin(\tilde{\theta}) \frac{\partial \delta y}{\partial \tau} - \frac{\partial \Phi_{11}}{\partial \tilde{r}}\right] \frac{\partial \zeta_0}{\partial \tilde{r}} \\ & + \zeta_0 \frac{\partial w_0}{\partial \tilde{z}} - w_0 \frac{\partial \zeta_0}{\partial \tilde{z}} - \tilde{r} \frac{\partial \Omega}{\partial \tilde{z}} \frac{\partial w_0}{\partial \tilde{r}}. \end{aligned} \tag{3.37}$$

The first two terms on the left-hand side of (3.37) come from the slow evolution of δx and δy. The third term is the advection of ζ_0 by the first-order potential flow.

https://doi.org/10.1017/jfm.2020.226 Published online by Cambridge University Press

The fourth term is the stretching of ζ_0. The fifth term comes from the vertical advection of ζ_0. The last term corresponds to the tilting of horizontal vorticity due to the vertical variation of the angular velocity. The solution, which is non-singular at $\tilde{r}=0$, can also be found by the method of variation of parameters as

$$\begin{aligned}\psi_{11} = & \left[\cos(\tilde{\theta})\frac{\partial \delta y}{\partial \tau} - \sin(\tilde{\theta})\frac{\partial \delta x}{\partial \tau}\right](\tilde{r}+\mu\tilde{r}\Omega)\\ & + \left[\cos(\tilde{\theta})\frac{\partial^2 \delta x}{\partial \tilde{z}^2} + \sin(\tilde{\theta})\frac{\partial^2 \delta y}{\partial \tilde{z}^2}\right](\psi_s+\alpha\tilde{r}\Omega)\\ & + t\cos(\tilde{\theta})(\psi_{p\Omega}+\lambda\tilde{r}\Omega)\frac{\mathrm{d}U}{\mathrm{d}\tilde{z}}\\ & - \Big[\sin(\tilde{\theta})\left(\lambda_0\tilde{r}\Omega+\lambda_1\tilde{r}+\psi_{ps}\right)+t\cos(\tilde{\theta})\left(\lambda_1\tilde{r}\Omega+\psi_{pc}\right)\\ & - \cos(\tilde{\theta})\left(\psi_{wc}+\tilde{r}\Omega\mathscr{C}_w-\tilde{r}\frac{\partial \mathscr{S}_w}{\partial t}\right)\\ & - \sin(\tilde{\theta})\left(\psi_{ws}+\tilde{r}\Omega\mathscr{S}_w+\tilde{r}\frac{\partial \mathscr{C}_w}{\partial t}\right)\Big]\frac{\mathrm{d}^2U}{\mathrm{d}\tilde{z}^2},\end{aligned} \tag{3.38}$$

where ψ_s, $\psi_{p\Omega}$, ψ_{ps} and ψ_{pc} are given in appendix C, while ψ_{wc} and ψ_{ws} will be defined later. The subscripts on these streamfunctions denote the same physical effects as for the potentials in (3.36). The parameters μ, α, λ, λ_0 and λ_1 are arbitrary functions of $\tilde{z}$ and τ, while $\mathscr{C}_w$ and $\mathscr{S}_w$ are arbitrary functions of $\tilde{z}$, τ and t. These functions are free because

$$\psi_h = \tilde{r}\Omega[\cos(\tilde{\theta})f(t)+\sin(\tilde{\theta})g(t)]+\tilde{r}[\sin(\tilde{\theta})f'(t)-\cos(\tilde{\theta})g'(t)] \tag{3.39}$$

is a homogeneous solution of (3.37) for any f and g depending on t. These solutions derive from the translational invariance (Billant 2010). In order to fix these parameters, we need to use a normalization condition. Here, we have chosen to impose that the mean displacement associated with the first-order vorticity $\nabla_h^2\psi_{11}$ is zero, i.e.

$$\int_0^{2\pi}\int_0^{+\infty} x\nabla_h^2\psi_{11}\tilde{r}\,\mathrm{d}\tilde{r}\,\mathrm{d}\tilde{\theta}=0, \quad \int_0^{2\pi}\int_0^{+\infty} y\nabla_h^2\psi_{11}\tilde{r}\,\mathrm{d}\tilde{r}\,\mathrm{d}\tilde{\theta}=0. \tag{3.40a,b}$$

In this way, only the displacements $U(\tilde{z})t+\delta x$ and δy of the leading-order vorticity ζ_0 will contribute to the mean displacement of the vortex. This will ease the comparison with the numerical simulations performed in Part 2, where the vortex displacements will be computed from vertical vorticity centroids. Hence, to enforce (3.40), we impose that

$$\langle\nabla_h^2\psi_{11},\tilde{r}\rangle \equiv \int_0^{+\infty}\nabla_h^2\psi_{11}\tilde{r}^2\,\mathrm{d}\tilde{r}=0. \tag{3.41}$$

In practice, we shall impose that each individual effect in (3.38) satisfies this condition. This leads to

$$\mu=0, \quad \lambda_1=-\alpha=\tfrac{1}{2}\langle\nabla_{\tilde{r}}^2\psi_{pc},\tilde{r}\rangle, \quad \lambda=\tfrac{1}{2}\langle\nabla_{\tilde{r}}^2\psi_{p\Omega},\tilde{r}\rangle, \quad \lambda_0=\tfrac{1}{2}\langle\nabla_{\tilde{r}}^2\psi_{ps},\tilde{r}\rangle, \tag{3.42a–d}$$

https://doi.org/10.1017/jfm.2020.226 Published online by Cambridge University Press

since $\langle \nabla^2_{\tilde{r}}(\tilde{r}\Omega), \tilde{r}\rangle = -2$, where the operator $\nabla^2_{\tilde{r}}$ is given by

$$\nabla^2_{\tilde{r}}\Lambda = \frac{\partial^2\Lambda}{\partial\tilde{r}^2} + \frac{1}{\tilde{r}}\frac{\partial\Lambda}{\partial\tilde{r}} - \frac{\Lambda}{\tilde{r}^2}, \tag{3.43}$$

for any function Λ. Finally, the two streamfunctions ψ_{wc} and ψ_{ws} associated with internal waves satisfy

$$\frac{\partial\nabla^2_{\tilde{r}}\psi_{wc}}{\partial t} + \Omega\nabla^2_{\tilde{r}}\psi_{ws} - \frac{1}{\tilde{r}}\frac{\partial\zeta_0}{\partial\tilde{r}}\psi_{ws} = -\frac{\partial\zeta_0}{\partial\tilde{r}}\frac{\partial\Phi_{wc}}{\partial\tilde{r}} - \zeta_0\nabla^2_{\tilde{r}}\Phi_{wc}, \tag{3.44}$$

$$\frac{\partial\nabla^2_{\tilde{r}}\psi_{ws}}{\partial t} - \Omega\nabla^2_{\tilde{r}}\psi_{wc} + \frac{1}{\tilde{r}}\frac{\partial\zeta_0}{\partial\tilde{r}}\psi_{wc} = -\frac{\partial\zeta_0}{\partial\tilde{r}}\frac{\partial\Phi_{ws}}{\partial\tilde{r}} - \zeta_0\nabla^2_{\tilde{r}}\Phi_{ws}, \tag{3.45}$$

where the potentials Φ_{wc} and Φ_{ws} are given by (B 2) and (B 3) in appendix B. Because the time and radial dependences in Φ_{wc} and Φ_{ws} are not separated, it is not possible to solve (3.44) and (3.45) analytically. We have therefore implemented a numerical resolution of (3.44) and (3.45). The time advancement is performed by a forward Euler scheme, spatial derivatives are computed by centred finite differences, and the Laplacian operator is inverted by means of the tridiagonal algorithm. The evolutions of Ω and ζ_0 over the slow time are taken into account through the numerical integration of equation (4.2), which will be derived later. The imposed boundary conditions are that $\psi_{ws} = \psi_{wc} = 0$ at $\tilde{r} = 0$ and that ψ_{ws} and ψ_{wc} vanish as $\tilde{r} \to +\infty$. Since the total streamfunction ψ_{11} defined in (3.38) should be zero at $t = \tau = 0$, the initial condition should be

$$\psi_{wc} = 0, \quad \psi_{ws} = -[\psi_{ps} + \lambda_0\tilde{r}\Omega + \lambda_1\tilde{r} - \vartheta(\tilde{z}, \tau = 0)\tilde{r}], \tag{3.46a,b}$$

since $\delta x = \delta y = \partial\delta x/\partial\tau = \partial\delta y/\partial\tau = 0$ at $\tau = 0$. The parameter $\vartheta(\tilde{z}, \tau = 0)$ is set such that $\psi_{ws} \to 0$ as $\tilde{r} \to +\infty$ initially, as required to integrate (3.44) and (3.45) numerically. From the expression (C 3) of ψ_{ps}, we have

$$\begin{aligned}\vartheta(\tilde{z}, \tau) \;=\; & \lambda_1(\tilde{z}, \tau) - \int_0^{+\infty} \mathscr{C}\left(\xi^2\Omega^2 F_h\mathscr{G} - \frac{1}{2}\right) \mathrm{d}\xi \\ & - \int_0^{+\infty} \frac{\zeta_0}{\eta^3\Omega^3}\int_0^{\eta} \xi^2\Omega^2\mathscr{C}\,\mathrm{d}\xi\,\mathrm{d}\eta,\end{aligned} \tag{3.47}$$

where $\mathscr{C}$ and $\mathscr{G}$ are defined in (3.25). There is no loss of generality in imposing that ψ_{ws} vanishes as $\tilde{r} \to +\infty$ initially because $\psi_{wh} = \vartheta t\tilde{r}\Omega\cos(\tilde{\theta}) + \vartheta\tilde{r}\sin(\tilde{\theta})$ is a homogeneous solution of (3.37). In other words, introducing the term $\vartheta\tilde{r}$ in ψ_{ws} is equivalent to substituting $\mathscr{C}_w$ by $\mathscr{C}_w + \vartheta t$ in (3.38). After the numerical integration, we enforce that the mean displacement associated to the internal waves is zero, yielding

$$\mathscr{C}_w(t, \tilde{z}, \tau) = \tfrac{1}{2}\langle\nabla^2_{\tilde{r}}\psi_{wc}, \tilde{r}\rangle, \quad \mathscr{S}_w(t, \tilde{z}, \tau) = \tfrac{1}{2}\langle\nabla^2_{\tilde{r}}\psi_{ws}, \tilde{r}\rangle. \tag{3.48a,b}$$

Figure 2(*a*,*b*) shows the streamfunctions ψ_{wc} and ψ_{ws} plotted against $\tilde{r}$ at different times, for $F_h = 0.1$ at $z = l_z/4$. In the next section, we will show that the angular velocity Ω does not evolve with τ in this plane. Hence, (3.44) and (3.45) have been integrated by imposing the initial angular velocity profile given by (2.11) for all time.

https://doi.org/10.1017/jfm.2020.226 Published online by Cambridge University Press

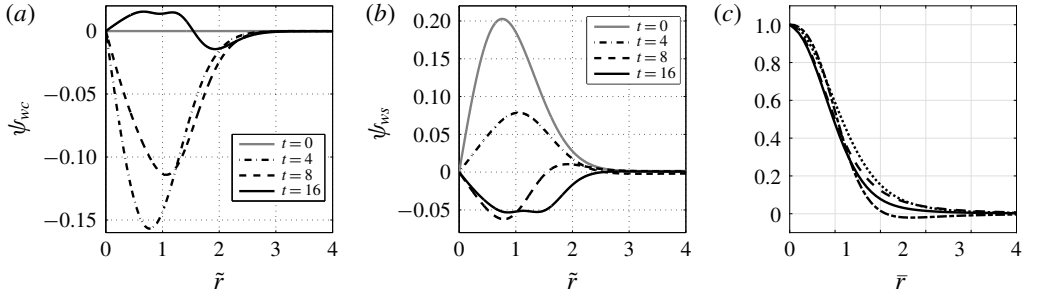


FIGURE 2. Streamfunctions (*a*) ψ_{wc} and (*b*) ψ_{ws} plotted against $\tilde{r}$ at $t=0$ (grey solid line), $t=4$ (black dash-dotted line), $t=8$ (black dashed line) and $t=16$ (black solid line), at $z=l_z/4$, where $\Omega=[1-\exp(-\tilde{r}^2)]/\tilde{r}^2$ regardless of τ. The Froude number is $F_h=0.1$. (*c*) Streamfunctions $\bar{\psi}_{2b}/(\beta_2\bar{r}^2)$ (solid line), $\bar{\psi}_{2s}/(\sigma_2\bar{r}^2)$ (dashed line), $\bar{\psi}_{2c}/(\chi_2\bar{r}^2)$ (dash-dotted line) and $\bar{\psi}^v_{2s}/(\sigma^v_2\bar{r}^2)$ (dotted line) computed in appendix D.

We see that, after an initial transient phase, the streamfunctions globally decay with time in the vortex core.

We have now fully determined the streamfunction at first order ψ_{11}. It satisfies the boundary condition at $\tilde{r}=0$. However, it can be shown that it behaves for large $\tilde{r}$ as

$$\begin{aligned}\psi_{11} \sim & \left[\cos(\tilde{\theta})\frac{\partial\delta y}{\partial\tau}-\sin(\tilde{\theta})\frac{\partial\delta x}{\partial\tau}\right]\tilde{r}\\ &+\frac{\mathscr{A}}{2}\left[\cos(\tilde{\theta})\frac{\partial^2\delta x}{\partial\tilde{z}^2}+\sin(\tilde{\theta})\frac{\partial^2\delta y}{\partial\tilde{z}^2}\right]\tilde{r}+\cos(\tilde{\theta})\frac{\mathscr{B}t}{2}\frac{\mathrm{d}U}{\mathrm{d}\tilde{z}}\tilde{r}\\ &+\left[-\sin(\tilde{\theta})\vartheta+\cos(\tilde{\theta})\frac{\mathscr{A}t}{2}+\cos(\tilde{\theta})\frac{\partial\mathscr{S}_w}{\partial t}-\sin(\tilde{\theta})\frac{\partial\mathscr{C}_w}{\partial t}\right]\frac{\mathrm{d}^2U}{\mathrm{d}\tilde{z}^2}\tilde{r},\end{aligned}\tag{3.49}$$

where $\mathscr{A}$ and $\mathscr{B}$ are given by

$$\mathscr{A}(\tilde{z},\tau)=\int_0^{+\infty}\xi^2\Omega^2\mathscr{C}\,\mathrm{d}\xi,\tag{3.50}$$

$$\mathscr{B}(\tilde{z},\tau)=\int_0^{+\infty}\xi^2\Omega\mathscr{C}\,(3+\mathscr{F})\,\frac{\partial\Omega}{\partial\tilde{z}}\,\mathrm{d}\xi\equiv\frac{\partial\mathscr{A}}{\partial\tilde{z}},\tag{3.51}$$

where $\mathscr{C}$ and $\mathscr{F}$ are defined in (3.25). Note that we have used the fact that ψ_{wc} and ψ_{ws} tend to zero as $\tilde{r}\to+\infty$.

In order to enforce the boundary condition $\psi_{11}\to 0$ as $\tilde{r}\to+\infty$, we need to impose

$$\frac{\partial\delta x}{\partial\tau}=\left[\frac{\mathscr{A}(\tilde{z},\tau)}{2}\frac{\partial^2\delta y}{\partial\tilde{z}^2}-\left(\vartheta(\tilde{z},\tau)+\frac{\partial\mathscr{C}_w}{\partial t}(t,\tilde{z},\tau)\right)\frac{\mathrm{d}^2U}{\mathrm{d}\tilde{z}^2}\right],\tag{3.52}$$

$$\frac{\partial\delta y}{\partial\tau}=-\left[\frac{\partial}{\partial\tilde{z}}\left(\frac{\mathscr{A}(\tilde{z},\tau)}{2}t\frac{\mathrm{d}U}{\mathrm{d}\tilde{z}}\right)+\frac{\mathscr{A}(\tilde{z},\tau)}{2}\frac{\partial^2\delta x}{\partial\tilde{z}^2}+\frac{\partial\mathscr{S}_w}{\partial t}(t,\tilde{z},\tau)\frac{\mathrm{d}^2U}{\mathrm{d}\tilde{z}^2}\right].\tag{3.53}$$

When $U=0$, these equations are identical to those found by Billant (2010) for the self-induction of an isolated vortex in stratified non-rotating fluids.

https://doi.org/10.1017/jfm.2020.226 Published online by Cambridge University Press

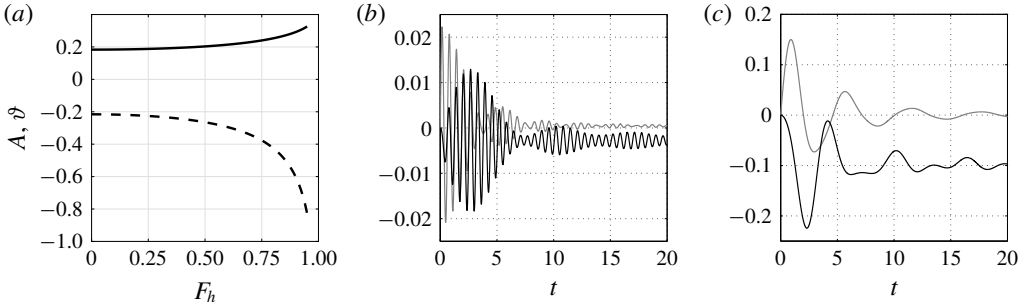


FIGURE 3. (*a*) Variables $\mathscr{A}$ (solid line) and ϑ (dashed line) plotted against F_h, at the vertical level $z = l_z/4$, where $\Omega = [1 - \exp(-\tilde{r}^2)]/\tilde{r}^2$ regardless of τ. (*b*,*c*) Forcings $\mathscr{C}_w$ (grey lines) and $\mathscr{S}_w$ (black lines) for (*b*) $F_h = 0.1$ and (*c*) $F_h = 0.5$, at $z = l_z/4$.

Figure 3(*a*) shows $\mathscr{A}$ and ϑ as functions of F_h at $z = l_z/4$, where the angular velocity remains the same, $\Omega = [1 - \exp(-\tilde{r}^2)]/\tilde{r}^2$, independent of τ (see § 4.1). They are almost independent of F_h for $F_h \lesssim 0.5$. The wave forcing terms $\mathscr{C}_w$ and $\mathscr{S}_w$ are also shown in figure 3(*b*,*c*) for two Froude numbers $F_h = 0.1$ and $F_h = 0.5$, at the same location. In appendix E, it is shown that they behave for small time as

$$\mathscr{C}_w = -\vartheta t + O(t^3), \quad \mathscr{S}_w = -\frac{\mathscr{A}}{4} t^2 + O(t^4). \tag{3.54a,b}$$

Therefore, they initially compensate the effect of the shear flow in (3.52) and (3.53). Then, they go through oscillations as seen in figure 3(*b*,*c*). These oscillations exhibit two typical periods: the non-dimensional period of rotation in the vortex core, $T \sim 2\pi$, and the buoyancy period, $T \sim 2\pi F_h$. For $F_h = 0.5$ (figure 3*c*), these two periods are comparable so that $\mathscr{C}_w$ and $\mathscr{S}_w$ exhibit irregular oscillations, while for $F_h = 0.1$ (figure 3*b*), fast oscillations superimposed on slow oscillations can be clearly distinguished. For large times, $\mathscr{C}_w$ and $\mathscr{S}_w$ tend to constant values because the waves are increasingly sheared by the vortex rotation through the terms $\cos(\Omega t - \tilde{\theta})$ and $\sin(\Omega t - \tilde{\theta})$ as seen in (3.23). As a result, their contributions $\partial\mathscr{C}_w/\partial t$ and $\partial\mathscr{S}_w/\partial t$ to the vortex displacements vanish as $t \to +\infty$.

In the next two sections, we will determine how the angular velocity evolves on the slow time τ. Then, (3.52) and (3.53) will be solved in §4.2.

3.2.2. *Determination of* (Φ_{10}, ψ_{10})

We now determine (Φ_{10}, ψ_{10}) corresponding to the azimuthal mode $m = 0$ of the potential and streamfunction at first order (3.32). In order to keep the calculations relatively simple, we will assume here that the Froude number is small so that the hydrostatic approximation is satisfied. The comparison with the DNS in Part 2 will show that this assumption provides accurate predictions at least for $F_h \leqslant 0.5$. We will therefore take the limit $F_h \to 0$ of the vertical velocity and buoyancy (3.23) and (3.24). In addition, equations (3.52) and (3.53) for the displacement perturbations derived in the previous section show that $(\delta x, \delta y)$ remain of order unity for large time $t = O(1/\varepsilon)$ and are therefore small compared to the terms growing like t. Therefore, these displacements will be neglected in (3.23) and (3.24) in order to

https://doi.org/10.1017/jfm.2020.226 Published online by Cambridge University Press

avoid lengthy calculations. Hence, (3.23) and (3.24) are simplified as follows:

$$w_0 = \left[\cos(\tilde{\theta}) - t\sin(\tilde{\theta})\Omega - \cos(\Omega t - \tilde{\theta})\cos\left(\frac{t}{F_h}\right)\right]\tilde{r}\Omega^2\frac{\mathrm{d}U}{\mathrm{d}\tilde{z}}, \tag{3.55}$$

$$b_0 = -t\cos(\tilde{\theta})\tilde{r}\Omega^2\frac{\mathrm{d}U}{\mathrm{d}\tilde{z}}. \tag{3.56}$$

The only remaining term due to internal waves is the third term in (3.55). The forcing terms in (3.33) and (3.34) for $m=0$ and $m=2$, i.e. $(\delta D_0, \delta D_2, \delta Z_0, \delta Z_2)$, have been derived using (3.55).

Equation (3.33) for the potential Φ_{10} reads

$$\nabla_h^2\Phi_{10} = \left[\frac{\partial\tilde{r}\Omega}{\partial\tilde{r}} - \left(\frac{\partial\tilde{r}\Omega}{\partial\tilde{r}}\cos(\Omega t) - \frac{t}{2}\tilde{r}\Omega\frac{\partial\Omega}{\partial\tilde{r}}\sin(\Omega t)\right)\cos\left(\frac{t}{F_h}\right)\right]\Omega t\left(\frac{\mathrm{d}U}{\mathrm{d}\tilde{z}}\right)^2. \tag{3.57}$$

The solution, which is not singular at $\tilde{r}=0$ and which vanishes at infinity, is

$$\Phi_{10} = \frac{t}{2}\left[\int_{+\infty}^{\tilde{r}}\xi\Omega^2\,\mathrm{d}\xi - \cos\left(\frac{t}{F_h}\right)\int_{+\infty}^{\tilde{r}}\xi\Omega^2\cos(\Omega t)\,\mathrm{d}\xi\right]\left(\frac{\mathrm{d}U}{\mathrm{d}\tilde{z}}\right)^2. \tag{3.58}$$

Using (3.58), equation (3.34) for the streamfunction ψ_{10} is

$$\mathrm{L}(\psi_{10}) = -\frac{\partial\zeta_0}{\partial\tau} + \mathscr{F}_{10}, \tag{3.59}$$

where

$$\mathscr{F}_{10} = \left[-\frac{t}{\tilde{r}}\frac{\partial\tilde{r}^2\Omega^3}{\partial\tilde{r}} - \left[\Omega\left(\frac{\partial\tilde{r}\Omega}{\partial\tilde{r}} + \frac{t^2}{2}\tilde{r}\Omega^2\frac{\partial\Omega}{\partial\tilde{r}}\right)\sin(\Omega t) - t\Omega^2\frac{\partial\tilde{r}\Omega}{\partial\tilde{r}}\cos(\Omega t)\right]\cos\left(\frac{t}{F_h}\right) + \frac{\tilde{\tau}^2}{2\tilde{R}e_b}\frac{1}{\tilde{r}}\frac{\partial}{\partial\tilde{r}}\left(\tilde{r}\frac{\partial\zeta_0}{\partial\tilde{r}}\right)\right]\left(\frac{\mathrm{d}U}{\mathrm{d}\tilde{z}}\right)^2, \tag{3.60}$$

where we remind the reader that $\tilde{\tau}=\varepsilon t$. Since ψ_{10} is axisymmetric, the operator L in (3.59) reduces to $\partial\nabla_h^2\psi_{10}/\partial t$. In addition, we should impose that

$$\left\langle\nabla_h^2\psi_{10}, \zeta_0\right\rangle = 0, \tag{3.61}$$

in order that the vertical vorticity at first order is orthogonal to the vertical vorticity at leading order. Taking the scalar product of (3.59) with ζ_0 shows that $\partial\langle\nabla_h^2\psi_{10}, \zeta_0\rangle/\partial t = 0$ only if

$$\frac{\partial\zeta_0}{\partial\tau} = \mathscr{F}_{10}. \tag{3.62}$$

This equation describes the evolution of the leading-order vertical vorticity of the vortex (and associated angular velocity) over the slow time. It is analysed in § 4.1. The potential and streamfunction (Φ_{12}, ψ_{12}) are solved in appendix D.

https://doi.org/10.1017/jfm.2020.226 Published online by Cambridge University Press

4. Results

4.1. *Evolution of the angular velocity of the vortex*

Here, we analyse in detail the evolution equation (3.62) of the leading-order vertical vorticity. By rescaling the slow time, the vertical coordinate and the buoyancy Reynolds number, and by integrating in $\tilde{r}$, we can derive from (3.62) an equation for the angular velocity Ω:

$$\frac{\partial \Omega}{\partial t} = \left[-F_h^2 t \Omega^3 + \frac{F_h^2 \Omega^2}{2} \left(\Omega t \cos(\Omega t) - \sin(\Omega t) \right) \cos\left(\frac{t}{F_h} \right) + \frac{t^2}{2Re\tilde{r}} \frac{\partial \zeta_0}{\partial \tilde{r}} \right] \left(\frac{\mathrm{d}U}{\mathrm{d}z} \right)^2 . \tag{4.1}$$

This equation shows that the angular velocity of the vortex decays because of dynamic and viscous effects (first and third terms on the right-hand side, respectively). The second term on the right-hand side corresponds to the effect of internal waves. However, we have observed that this effect is always weak. To illustrate this point, figure 5(*c*) (later in this section) shows that the angular velocity at the centre computed from (4.1) (black solid lines) is very close to the one computed by neglecting them (red lines), i.e. from

$$\frac{\partial \Omega}{\partial t} = \left[-F_h^2 t \Omega^3 + \frac{t^2}{2Re\tilde{r}} \frac{\partial \zeta_0}{\partial \tilde{r}} \right] \left(\frac{\mathrm{d}U}{\mathrm{d}z} \right)^2 . \tag{4.2}$$

We will therefore use this simplified equation in the following.

By equating the magnitude of the different terms in (4.2), it can be noticed that the intrinsic time scale of the equation is $\tilde{\tau} = \varepsilon t$ if the buoyancy Reynolds number scales as $ReF_h^2 = O(1/\varepsilon)$. However, it is not possible to perform a rigorous asymptotic analysis based on this time scale, as discussed in appendix A.

A physical interpretation of the origin of the dynamic effect (first term on the right-hand side of (4.2)) can be gained by considering the conservation of potential vorticity near the vortex axis when the vortex becomes tilted. First, let us consider the buoyancy at leading order $b = \varepsilon b_0 / F_h = -t\tilde{x}\Omega^2 \, \mathrm{d}U/\mathrm{d}z$, where b_0 is given by (3.56) and $\tilde{x} = x - U(z)t$ (we neglect δx). Figure 4 sketches the lines of constant total buoyancy $b_t = b + z/F_h^2$ near the point $x = 0$, $z = l_z/2$ at two times: $t = 0$ (grey dashed lines) and $t = t_0$ (grey solid lines) where t_0 is small. At $t = t_0$, the vortex axis $\tilde{x} = 0$ (bold solid line) is inclined towards the left since $x = U(z)t_0 \simeq -k_z U_S t_0 (z - l_z/2)$ near $z = l_z/2$. The iso-buoyancy lines are also no longer horizontal but slanted downwards towards the positive x direction. On the vortex axis $\tilde{x} = 0$, they remain at the same vertical level, while on the line $x = 0$, they are displaced by

$$\delta h = -F_h^2 \Omega^2 h t_0^2 \left(\frac{\mathrm{d}U}{\mathrm{d}z} \right)^2 , \tag{4.3}$$

where $h = z_0 - l_z/2$ with z_0 the initial vertical level of the iso-buoyancy line. Therefore δh is negative, as clearly seen in figure 4. Since the vortex is inclined, the iso-buoyancy lines are indeed displaced towards the vortex axis where the pressure is minimum. This means that the vortex is squeezed near $x = 0$, $z = l_z/2$. The conservation of potential vorticity between the iso-density lines at $z = z_0$ and $z = l_z/2$ (figure 4),

$$\frac{\zeta}{h} = \frac{\zeta + \delta\zeta}{h + \delta h}, \tag{4.4}$$

https://doi.org/10.1017/jfm.2020.226 Published online by Cambridge University Press

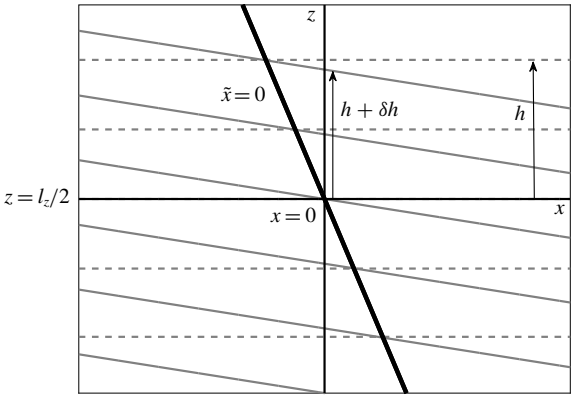


FIGURE 4. Lines of constant total buoyancy b_t near the point $x=0$, $z=l_z/2$ at $t=0$ (grey dashed lines) and $t=t_0$ (grey solid lines). The bold black solid line represents the vortex axis at $t=t_0$. Here δh is the height variation at $x=0$ of the iso-buoyancy line located at $z=h+l_z/2$ initially.

implies that the vertical vorticity at $t=t_0$ will decrease by $\delta\zeta=\zeta\delta h/h$. The variation of vertical vorticity between $t=0$ and $t=t_0$ is therefore

$$\frac{\partial\zeta}{\partial t}=\frac{\delta\zeta}{t_0}=-F_h^2\zeta\Omega^2 t_0\left(\frac{\mathrm{d}U}{\mathrm{d}z}\right)^2. \tag{4.5}$$

This corresponds exactly to (4.2) for $Re=\infty$ since $\zeta=2\Omega$ on the vortex axis. However, we stress that (4.2) is valid not only on the vortex axis near $z=l_z/2$ but everywhere.

Both the dynamic and viscous decay of Ω are proportional to $(\mathrm{d}U/\mathrm{d}z)^2$. Hence, the decay will be maximum at $z=0, l_z/2$ and will vanish at $z=l_z/4$ and $3l_z/4$ for the sinusoidal profile $U=U_S\sin(k_z z)$. This explains why we have taken the initial angular velocity profile for computing the quantities at $z=l_z/4$ shown in figures 2 and 3.

Equation (4.2) can be solved by a multiple scale analysis. To do so, we introduce the time $\tilde{t}=(F_h t|\mathrm{d}U/\mathrm{d}z|)^3$. Then, (4.2) becomes

$$\frac{\partial\Omega}{\partial\tilde{t}}=-\frac{\Omega^3}{3\tilde{t}^{1/3}}+\frac{\gamma}{6\tilde{r}}\frac{\partial\zeta_0}{\partial\tilde{r}},\quad \text{where } \gamma=1\Big/\left(ReF_h^3\left|\frac{\mathrm{d}U}{\mathrm{d}z}\right|\right) \tag{4.6}$$

is the only remaining control parameter. For a given set of parameters (F_h, Re, k_z, U_S), γ lies between $1/(ReF_h^3 k_z U_S)$ and infinity as the vertical coordinate varies. For small γ, the solution can be found as (appendix F.1)

$$\Omega=\frac{\Omega_i}{\sqrt{1+\tilde{t}^{2/3}\Omega_i^2}}-\frac{\gamma}{2}\left(\frac{\partial\Omega_i}{\partial\tilde{r}}\right)^2\frac{3\arctan(\Omega_i\tilde{t}^{1/3})-3\tilde{t}^{1/3}\Omega_i+\tilde{t}\Omega_i^3}{\Omega_i^4\left(1+\tilde{t}^{2/3}\Omega_i^2\right)^{3/2}}+O(\gamma^2), \tag{4.7}$$

with

$$\Omega_i=\frac{1}{\tilde{r}^2}\left[1-\exp\left(-\frac{\tilde{r}^2}{1+2\gamma\tilde{t}/3}\right)\right]. \tag{4.8}$$

https://doi.org/10.1017/jfm.2020.226 Published online by Cambridge University Press

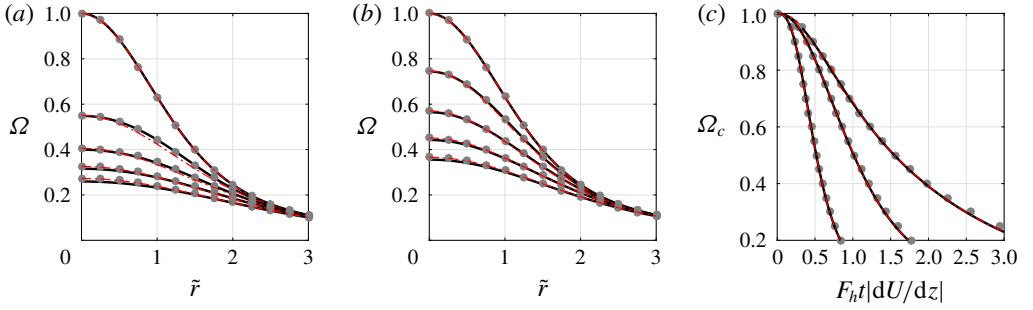


FIGURE 5. (*a,b*) Angular velocity profile Ω as a function of $\tilde{r}$ computed numerically from (4.6) (black solid lines) and predicted by (4.7) (grey circles) at different times for (*a*) $\gamma = 0.1$ and (*b*) $\gamma = 1$. The Lamb–Oseen profile (4.11) is also represented by red dash-dotted lines. The times shown are (*a*) $\tilde{t} = 0$, $\tilde{t} = 2.65$, $\tilde{t} = 7.50$, $\tilde{t} = 13.8$, $\tilde{t} = 21.2$ and (*b*) $\tilde{t} = 0$, $\tilde{t} = 0.265$, $\tilde{t} = 0.750$, $\tilde{t} = 1.38$, $\tilde{t} = 2.12$, from top to bottom. (*c*) Evolution of the angular velocity at the vortex centre Ω_c as a function of $\tilde{t}^{1/3} = F_h t|\mathrm{d}U/\mathrm{d}z|$ predicted by (4.10) (grey circles) and computed numerically from (4.6) (black solid lines) for $\gamma = 0.1$, $\gamma = 1$ and $\gamma = 10$ (top to bottom). The red dash-dotted lines represent the numerical integration of the full equation (4.1) for $F_h = 0.5$, $k_z = 1$ and $U_S = 0.2$.

This approximation is only valid in the time range $\tilde{t} \ll 1/\gamma^3$. However, there is no particular interest in studying the solution for $\tilde{t} > 1/\gamma^3$ when $\gamma \ll 1$ because, as shown in § 4.3, the shear is maximum when $\tilde{t} = O(1/\gamma)$, i.e. in the first time range $\tilde{t} \ll 1/\gamma^3$. Equation (4.7) implies that the angular velocity at the vortex centre evolves as

$$\Omega_c = 1/\sqrt{(1 + 2\gamma\tilde{t}/3)^2 + \tilde{t}^{2/3}} + O(\gamma^2), \tag{4.9}$$

i.e. in terms of t and the original parameters,

$$\Omega_c = 1 \Bigg/ \sqrt{\left[1 + \frac{2t^3}{3Re}\left(\frac{\mathrm{d}U}{\mathrm{d}z}\right)^2\right]^2 + F_h^2 t^2 \left(\frac{\mathrm{d}U}{\mathrm{d}z}\right)^2}. \tag{4.10}$$

In § F.2, we derive an approximation of the solution of (4.6) in the opposite limit: $\gamma \gg 1$. In this case, the angular velocity at leading order is given by $\Omega = \Omega_i$, where Ω_i is defined in (4.8). However, the expressions (4.9) and (4.10) of Ω_c derived for $\gamma \ll 1$ turn out to be valid at leading order also when $\gamma \gg 1$. Therefore, (4.10) will be used in the following and in Part 2 to describe the evolution of Ω_c regardless of the value of γ.

Figure 5(*a,b*) compares the asymptotic solution (4.7) to the numerical solution of (4.6) at different times $\tilde{t}$. We see that the agreement is excellent for $\gamma = 0.1$ (figure 5*a*) and even for $\gamma = 1$ (figure 5*b*). There are only some slight discrepancies in the vortex core $\tilde{r} \lesssim 1$ when $\tilde{t} \gtrsim 1$. In figure 5, the Lamb–Oseen profile

$$\Omega_e = \frac{1 - \exp(-\tilde{r}^2/\tilde{a}_e^2)}{\tilde{r}^2}, \tag{4.11}$$

with $\tilde{a}_e^2 = 1/\Omega_c$, where Ω_c is given by (4.10), has also been plotted with black dash-dotted lines. This profile is close to the asymptotic solution (4.7). This is the reason

https://doi.org/10.1017/jfm.2020.226 Published online by Cambridge University Press

why the empirical profile (4.11) is used in appendix D to ease the numerical resolution of the streamfunction ψ_{12}.

Figure 5(*c*) shows the asymptotic angular velocity at the vortex centre (4.10) and the numerical solution of (4.6) for different values of the control parameter γ. The agreement is very good not only for $\gamma = 0.1$ but also for $\gamma = 1$ and for $\gamma = 10$, confirming that (4.10) is a valid approximation of Ω_c whatever the magnitude of γ.

4.2. *Analysis of the vortex deformations*

Having determined the evolution of Ω, we now come back to the study of equations (3.52) and (3.53) for the vortex displacements.

4.2.1. *General solution*

To solve (3.52) and (3.53), it is first convenient to rescale the slow time τ in terms of the time t:

$$\frac{\partial \delta x}{\partial t} = \left[\frac{\mathscr{A}(\tilde{z},t)}{2}\frac{\partial^2 \delta y}{\partial \tilde{z}^2} - \left(\vartheta(\tilde{z},t) + \frac{\partial \mathscr{C}_w}{\partial t}(\tilde{z},t)\right)\frac{\mathrm{d}^2 U}{\mathrm{d}\tilde{z}^2}\right]\varepsilon^2, \tag{4.12}$$

$$\frac{\partial \delta y}{\partial t} = -\left[\frac{\partial}{\partial \tilde{z}}\left(\frac{\mathscr{A}(\tilde{z},t)}{2}t\frac{\mathrm{d}U}{\mathrm{d}\tilde{z}}\right) + \frac{\mathscr{A}(\tilde{z},t)}{2}\frac{\partial^2 \delta x}{\partial \tilde{z}^2} + \frac{\partial \mathscr{S}_w}{\partial t}(\tilde{z},t)\frac{\mathrm{d}^2 U}{\mathrm{d}\tilde{z}^2}\right]\varepsilon^2. \tag{4.13}$$

The solution of (4.12) and (4.13) can be decomposed as

$$\delta x = \delta x^* - \varepsilon^2\left[\mathscr{C}_w + \int_0^t \vartheta(\tilde{z},\upsilon)\,\mathrm{d}\upsilon\right]\frac{\mathrm{d}^2 U}{\mathrm{d}\tilde{z}^2}, \tag{4.14}$$

$$\delta y = \delta y^* - \varepsilon^2\left[\mathscr{S}_w\frac{\mathrm{d}^2 U}{\mathrm{d}\tilde{z}^2} + \int_0^t \frac{\partial}{\partial \tilde{z}}\left(\frac{\mathscr{A}(\tilde{z},\upsilon)}{2}\frac{\mathrm{d}U}{\mathrm{d}\tilde{z}}\right)\upsilon\,\mathrm{d}\upsilon\right], \tag{4.15}$$

giving

$$\frac{\partial \delta x^*}{\partial t} = \hat{\omega}\frac{\partial^2 \delta y^*}{\partial \tilde{z}^2} + O(\varepsilon^4), \tag{4.16}$$

$$\frac{\partial \delta y^*}{\partial t} = -\hat{\omega}\frac{\partial^2 \delta x^*}{\partial \tilde{z}^2} + O(\varepsilon^4), \tag{4.17}$$

where $\hat{\omega} = \varepsilon^2\mathscr{A}/2$. Since (4.12) and (4.13) are valid up to order $O(\varepsilon^2)$, it is indeed legitimate to neglect the terms $O(\varepsilon^4)$ in (4.16) and (4.17). Since $\hat{\omega}$ is small, an approximation of the solution of (4.16) and (4.17) can be found in the form

$$\delta x^* = \mathrm{e}^{\mathrm{i}\tilde{k}_z\tilde{z}}\left[\delta x_c^* \cos\left(\int_0^t \hat{\omega}(z,\upsilon)\,\mathrm{d}\upsilon\right) + \delta x_s^* \sin\left(\int_0^t \hat{\omega}(z,\upsilon)\,\mathrm{d}\upsilon\right)\right] + \text{c.c.}, \tag{4.18}$$

$$\delta y^* = \mathrm{e}^{\mathrm{i}\tilde{k}_z\tilde{z}}\left[-\delta x_s^* \cos\left(\int_0^t \hat{\omega}(z,\upsilon)\,\mathrm{d}\upsilon\right) + \delta x_c^* \sin\left(\int_0^t \hat{\omega}(z,\upsilon)\,\mathrm{d}\upsilon\right)\right] + \text{c.c.}, \tag{4.19}$$

where δx_c^* and δx_s^* are constants. The initial conditions $\delta x = \delta y = 0$ at $t = 0$ impose $\delta x_c^* = \delta x_s^* = 0$. Therefore, a solution of (4.12) and (4.13) valid up to order $O(\varepsilon^2)$ is

$$\delta x = -\varepsilon^2\left[\mathscr{C}_w + \int_0^t \vartheta(\tilde{z},\upsilon)\,\mathrm{d}\upsilon\right]\frac{\mathrm{d}^2 U}{\mathrm{d}\tilde{z}^2}, \tag{4.20}$$

https://doi.org/10.1017/jfm.2020.226 Published online by Cambridge University Press

$$\delta y = -\varepsilon^2 \left[\mathscr{S}_w \frac{\mathrm{d}^2 U}{\mathrm{d}\tilde{z}^2} + \int_0^t \frac{\partial}{\partial \tilde{z}} \left(\frac{\mathscr{A}(\tilde{z}, \upsilon)}{2} \frac{\mathrm{d}U}{\mathrm{d}\tilde{z}} \right) \upsilon \, \mathrm{d}\upsilon \right]. \tag{4.21}$$

These equations show that the vortex axis evolves because of three different effects in addition to the advection $U t \boldsymbol{e}_x$ by the shear flow:

(i) the displacement due to internal waves (first terms on the right-hand side of (4.20) and (4.21));

(ii) the second term on the right-hand side of (4.20), which describes a small delay (since ϑ is negative as seen in figure 3*a*) in the advection by the shear flow due to its vertical variations;

(iii) the self-induction (second term on the right-hand side of (4.21)) – the shear flow bends the vortex in the x direction and, in turn, this creates a self-induced motion in the y direction; this effect is modulated along the vertical since $\mathscr{A}$ varies via the vertical variation of the angular velocity of the vortex.

For large time such that $\tilde{\tau} = \varepsilon t = O(1)$, (4.20) and (4.21) reduce at leading order to

$$\delta x = -\varepsilon \int_0^{\tilde{\tau}} \vartheta \, \mathrm{d}\upsilon \, \frac{\mathrm{d}^2 U}{\mathrm{d}\tilde{z}^2}, \tag{4.22}$$

$$\delta y = -\int_0^{\tilde{\tau}} \frac{\partial}{\partial \tilde{z}} \left(\frac{\mathscr{A}}{2} \frac{\mathrm{d}U}{\mathrm{d}\tilde{z}} \right) \upsilon \, \mathrm{d}\upsilon, \tag{4.23}$$

where we remind the reader that ϑ and $\mathscr{A}$ are defined in (3.47) and (3.50). These expressions show that the displacements are $\delta y = O(1)$, while $\delta x = O(\varepsilon)$ for $t \sim 1/\varepsilon$. The effect of internal waves remains $O(\varepsilon^2)$ and is thus negligible. This is the reason why we have neglected $(\delta x, \delta y)$ compared to $U(\tilde{z})t$ in § 3.2.2.

4.2.2. *Behaviour for small time*

By substituting $\mathscr{C}_w$ and $\mathscr{S}_w$ in (4.20) and (4.21) by their asymptotic expressions (E 12) derived for small time (see appendix E) and by assuming that the angular velocity does not evolve for small time, we find that the displacements behave for $t \ll 1$ as

$$\delta x = k_z^2 \varsigma t^3 \frac{\mathrm{d}^2 U}{\mathrm{d}\tilde{z}^2} + O(t^4), \quad \delta y = k_z^2 \sigma t^4 \frac{\mathrm{d}^2 U}{\mathrm{d}\tilde{z}^2} + O(t^5), \tag{4.24a,b}$$

where ς and σ are constants given in (E 13).

Remarkably, the initial evolution of $(\delta x, \delta y)$ is independent of the Froude number at leading order. At this order, δx and δy vary like t^3 and t^4, respectively. It is interesting to compare the predictions (4.24) to those of a heuristic model where the advection by the shear flow is directly added to the equations of the self-induced motion of the single vortex, i.e.

$$\frac{\partial \Delta x}{\partial t} = \hat{\omega} \frac{\partial^2 \delta y}{\partial \tilde{z}^2} + U(\tilde{z}), \tag{4.25}$$

$$\frac{\partial \delta y}{\partial t} = -\hat{\omega} \frac{\partial^2 \Delta x}{\partial \tilde{z}^2}, \tag{4.26}$$

where $\Delta x = U(\tilde{z})t + \delta x$ is the total displacement of the vortex in the streamwise direction. Such a phenomenological model can be obtained from (4.12) and (4.13)

https://doi.org/10.1017/jfm.2020.226 Published online by Cambridge University Press

by setting $\partial\mathscr{C}_w/\partial t = \partial\mathscr{S}_w/\partial t = \vartheta = 0$ and $\partial\Omega_c/\partial\tilde{z} = 0$, i.e. by neglecting the effect of the waves, the three-dimensional correction of the advection by the base flow and by assuming that the angular velocity remains constant with time. The model (4.25) and (4.26) has been introduced, for example, by Marshall & Parthasarathy (1993) for two-layer quasi-geostrophic flows. For small times $t \ll 1$, the solution of (4.25) and (4.26) is

$$\delta x = -\frac{\hat{\omega}^2}{6}t^3\frac{\mathrm{d}^4U}{\mathrm{d}\tilde{z}^4} + O(t^4), \quad \delta y = -\frac{\hat{\omega}}{2}t^2\frac{\mathrm{d}^2U}{\mathrm{d}\tilde{z}^2} + O(t^3). \tag{4.27a,b}$$

Thus, δx is initially of order $k_z^4F_h^4t^3$ instead of $k_z^2t^3$, and δy is of order $k_z^2F_h^2t^2$ instead of $k_z^2t^4$. This shows that internal waves have an important effect on the initial dynamics of the vortex. (Note, however, that such waves should be absent in the quasi-geostrophic limit considered by Marshall & Parthasarathy (1993).)

4.3. *Evolution of the Richardson number*

From the asymptotic expressions of the velocity and buoyancy fields, it is now possible to predict the evolution of the Richardson number:

$$Ri = \frac{\dfrac{1}{F_h^2} + \dfrac{\partial b}{\partial z}}{\left(\dfrac{\partial u}{\partial z}\right)^2 + \left(\dfrac{\partial v}{\partial z}\right)^2}. \tag{4.28}$$

In the DNS performed in Part 2, we will see that the Richardson number reaches its minimum or the Kelvin–Helmholtz instability first appears at the vortex centre $\tilde{r} = 0$ and at the levels $z = 0$ and $l_z/2$ where the ambient shear is maximum. In the following, we will therefore focus on the point $(\tilde{r} = 0,\ z = l_z/2)$ (the point $(\tilde{r} = 0,\ z = 0)$ is equivalent due to the symmetry of the ambient shear flow).

The vertical shear of the horizontal velocity at this location can be computed by using the expansion of the velocity field (3.4) and the expression of the total derivative (3.12) (or (3.19)). This leads to

$$\begin{aligned}\frac{\partial u_c}{\partial z} &= k_zU_S^3\varepsilon^2t\left[\left(\frac{3}{4}-\sigma_2\right)t\Omega_c^2 - \frac{\sigma_2^\nu t^2\Omega_c}{ReF_h^2}\right] + \Omega_c\frac{\partial\delta y_c}{\partial z}\\ &\quad - k_zU_S + k_z\varepsilon^2U_S\left(\mathscr{D}_c + \lambda_{0c}\Omega_c + \lambda_{1c} - \vartheta_c\right),\end{aligned} \tag{4.29}$$

$$\begin{aligned}\frac{\partial v_c}{\partial z} &= k_zU_St\Omega_c - k_zU_S^3\varepsilon^2t\left[\beta_2\Omega_c + \left(\frac{1}{4}+\chi_2\right)t^2\Omega_c^3\right] - \Omega_c\frac{\partial\delta x_c}{\partial z}\\ &\quad - k_zU_St\left[\varepsilon^2\left(\lambda_{1c}\Omega_c + \mathscr{D}_c\Omega_c + \frac{\mathscr{A}_c}{2}\right)\right.\\ &\quad \left. - \frac{F_h^2}{2}\frac{\partial^2\mathscr{A}_c}{\partial z^2} - F_h^2\Omega_c\left(\frac{3}{2}\frac{\partial^2\mathscr{D}_c}{\partial z^2} - \frac{\partial\lambda_c}{\partial z}\right)\right],\end{aligned} \tag{4.30}$$

where the subscript c indicates that the values are computed at $(\tilde{r} = 0,\ z = l_z/2)$ or $z = l_z/2$ for the quantities independent of $\tilde{r}$. The terms in the first line on the right-hand sides of (4.29) and (4.30) come from the horizontal derivatives, while those in the next lines originate from the vertical derivative at constant horizontal coordinates

https://doi.org/10.1017/jfm.2020.226 Published online by Cambridge University Press

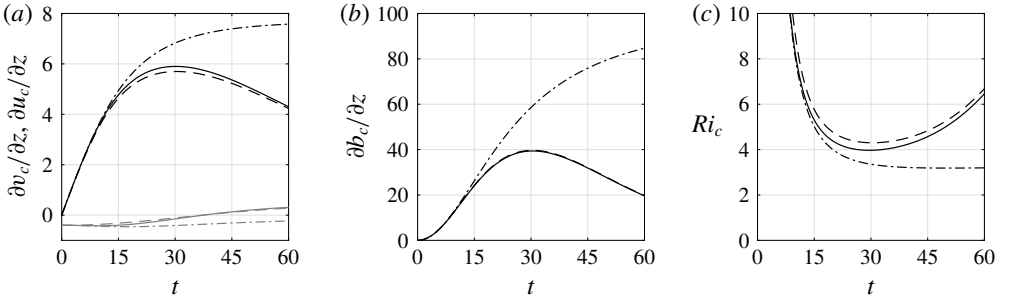


FIGURE 6. Evolution of (*a*) $\partial u_c/\partial z$ (grey lines) and $\partial v_c/\partial z$ (black lines), (*b*) $\partial b/\partial z$ and (*c*) Ri_c predicted by (4.29), (4.30) and (4.32) for $F_h = 0.1$, $k_z = 2$, $U_S = 0.2$ and for $Re = 6000$ (solid lines) and $Re = \infty$ (dash-dotted lines). The dashed lines represent the predictions from the approximations (4.33), (4.34), (4.35) and (4.36).

(see (3.12)). The terms of order ε^4 have been neglected. In particular, the fact that $(\delta x, \delta y)$ are formally of order ε^2 (see (4.20) and (4.21)) has been used. The internal waves have been omitted in (4.29) and (4.30) for the reasons explained in § 3.1. The coefficients β_2, σ_2, χ_2 and σ_2^v are given in equations (D 15). The parameters $(\lambda_0, \lambda_1, \lambda)$, ϑ and $\mathscr{A}$ are defined in (3.42), (3.47) and (3.50), respectively. The parameter $\mathscr{D}$ is

$$\mathscr{D} = \int_0^{+\infty} \xi\, \Omega^2 \, \mathrm{d}\xi. \tag{4.31}$$

Similarly, the total vertical derivative of the buoyancy at $\tilde{r} = 0$, $z = l_z/2$ can be obtained from the leading-order expression of the buoyancy in the hydrostatic limit (3.56):

$$\frac{\partial b_c}{\partial z} = \left(k_z U_S t - \frac{\partial \delta x_c}{\partial z} \right) k_z U_S t \Omega_c^2. \tag{4.32}$$

Figure 6(*a*,*b*) shows one example of the evolution of $\partial u_c/\partial z$, $\partial v_c/\partial z$ and $\partial b_c/\partial z$ predicted by (4.29), (4.30) and (4.32) (solid lines). They all reach a maximum value at a finite time. Remarkably, the magnitude of $\partial u_c/\partial z$ is much lower than $\partial v_c/\partial z$. As seen in figure 6(*c*), the corresponding Richardson number Ri_c reaches a minimum value approximately equal to 4. In the inviscid limit, represented by dash-dotted lines, $\partial v_c/\partial z$, $\partial b_c/\partial z$ and Ri_c saturate to finite values as $t \to \infty$. The saturation of $\partial v_c/\partial z$ is intimately linked to the decay of the angular velocity of the vortex due to the squeezing of the isopycnal surfaces and potential vorticity conservation. The same effect is responsible for the growth and saturation of $\partial b_c/\partial z$.

To study the extrema of the quantities (4.29), (4.30) and (4.32), it is convenient to rewrite them as

$$\frac{\partial u_c}{\partial z} = \frac{\varepsilon U_S}{F_h} \left[-1 + \left(\frac{3}{4} - \sigma_2 \right) \eta^2 - \frac{\sigma_2^v \eta^3 \gamma_c}{\Omega_c^2} + O(\varepsilon^2) \right], \tag{4.33}$$

$$\frac{\partial v_c}{\partial z} = \frac{\eta}{F_h} \left[1 - \left(\frac{1}{4} + \chi_2 \right) \eta^2 + O(\varepsilon^2) \right], \tag{4.34}$$

$$\frac{\partial b_c}{\partial z} = \frac{\eta^2}{F_h^2} \left[1 + O(\varepsilon^2) \right], \tag{4.35}$$

https://doi.org/10.1017/jfm.2020.226 Published online by Cambridge University Press

where $\eta = \varepsilon U_S t \Omega_c$ and $\gamma_c = \gamma(z = l_z/2) = 1/(ReF_h^3 k_z U_S)$. This shows that $\partial v_c/\partial z$ and $\partial b_c/\partial z$ depend on time only through η at leading order in ε. We see also that $\partial u_c/\partial z$ is one order in ε smaller than $\partial v_c/\partial z$ and $\partial b_c/\partial z$ for $\eta = O(1)$. We can notice that the last two terms of (4.34) are of order unity when $\eta = O(1)$. They are therefore of the same order as the leading-order term, although they originate from first-order terms in the asymptotic analysis (i.e. $O(\varepsilon^2)$). This clearly shows that the asymptotic analysis is non-uniform in time.

These approximations imply that, at leading order in ε, Ri_c reads as

$$Ri_c = \frac{1+\eta^2}{\eta^2[1-(\frac{1}{4}+\chi_2)\eta^2]^2}. \tag{4.36}$$

As seen by the dashed lines in figure 6, the approximations (4.33)–(4.36) are very close to the full predictions by (4.29)–(4.32).

The approximations (4.34)–(4.36) show that the three quantities $\partial v_c/\partial z$, $\partial b_c/\partial z$ and Ri_c reach their extrema when $\mathrm{d}\eta/\mathrm{d}t = 0$, giving the time

$$T_m = \varepsilon U_S t_m = \left(\frac{3}{4\gamma_c}\right)^{1/3} \tag{4.37}$$

by using (4.10). This shows that the long-wavelength assumption $\varepsilon U_S t < 1$ is expected to be all the more valid at the extremum than γ_c is large. It is also interesting to remark that t_m is independent of the Froude number: $t_m = (3Re)^{1/3}(2k_z U_S)^{-2/3}$. However, if the buoyancy Reynolds number $Re_b = ReF_h^2$ is assumed constant, a dependence on F_h is recovered since $t_m = (3Re_b)^{1/3}(2k_z F_h U_S)^{-2/3}$. At $t = t_m$, we have

$$\eta_m = \left(\frac{3}{4\gamma_c}\right)^{1/3} \Bigg/ \sqrt{\frac{9}{4} + \left(\frac{3}{4\gamma_c}\right)^{2/3}}. \tag{4.38}$$

When γ_c decreases from large values to zero (inviscid limit), η_m varies from $\eta_m \sim \gamma_c^{-1/3}$ to $\eta_m = 1$. Hence, for large γ_c, we have

$$\max\left(\frac{\partial v_c}{\partial z}\right) \sim (k_z U_S Re)^{1/3}, \quad \max\left(\frac{\partial b_c}{\partial z}\right) \sim (k_z U_S Re)^{2/3}, \quad \min(Ri_c) \sim \gamma_c^{2/3}, \tag{4.39a–c}$$

while in the inviscid limit we have

$$\max\left(\frac{\partial v_c}{\partial z}\right) \propto \frac{1}{F_h}, \quad \max\left(\frac{\partial b_c}{\partial z}\right) = \frac{1}{F_h^2}, \quad \min(Ri_c) = \frac{2}{(\frac{3}{4}-\chi_2)^2} = 3.46, \tag{4.40a–c}$$

For arbitrary η_m in the range $0 \leqslant \eta_m \leqslant 1$, it can be shown from (4.36) that $\min(Ri_c)$ is bounded: $\min(Ri_c) > 3.43$. This overall minimum is reached when $\eta_m^2 = -[3 + \sqrt{9 + 8/(1/4+\chi_2)}]/4 = 0.936$, i.e. close to the inviscid limit. This demonstrates that $\min(Ri_c)$ cannot go below the threshold $Ri = 0.25$ when $k_z F_h \ll 1$.

5. Conclusion

We have carried out an asymptotic analysis of the evolution of a columnar vortex in an ambient stratified shear flow for long wavelength. The vortex has initially a Lamb–Oseen profile, while the shear flow is horizontally uniform and varies sinusoidally

https://doi.org/10.1017/jfm.2020.226 Published online by Cambridge University Press

along the vertical: $U(z) = U_S \sin(k_z z)$. The Froude number F_h has been assumed to be lower than unity so that there is no critical layer where the angular velocity of the vortex is equal to the buoyancy frequency. The Reynolds number has been considered large.

An underlying assumption of the analysis is that the rescaled vertical wavenumber $k_z F_h$ is small. This particular parameter derives from the self-similarity of strongly stratified flows according to which the vertical wavenumber always appears multiplied by the Froude number F_h in the Euler equations under the Boussinesq approximation.

This asymptotic analysis provides governing equations for the displacement of the vortex axis and for its angular velocity. The vortex axis is advected by the shear flow at leading order $\Delta x = U(z)t$, but three different effects influence its trajectory at order $(k_z F_h)^2$ (see (4.20) and (4.21)). First, the vortex axis deviates perpendicularly to the direction of the shear flow owing to the self-induction of the vortex when it is bent. Second, internal waves, which are generated at the start-up of the motion, influence the initial evolution of the vortex. These waves oscillate at the buoyancy frequency N and make the dynamics initially non-hydrostatic. Later, their effects on the vortex trajectory quickly decay. It should be pointed out that these internal waves would be weaker if the shear flow were added smoothly to the vortex instead of instantaneously as done herein. The third effect is a three-dimensional effect that slightly reduces the advection in the direction of the shear flow.

The angular velocity of the vortex decreases with time because of dynamic and viscous effects (see (4.2) and (4.10)), while internal waves have a negligible effect on its evolution. The dynamic effect is due to the squeezing of the isopycnal surfaces when the vortex is inclined. To conserve potential vorticity, the core vertical vorticity therefore has to decrease. The viscous decay of the angular velocity is also quickly enhanced since the vertical shear increases algebraically with time. These two effects are not uniform along the vertical: they are maximum in the regions of high shear and vanish at the vertical levels where the shear is zero.

In addition, a horizontal velocity field with an azimuthal wavenumber $m = 2$ arises at order $(k_z F_h)^2$ (see appendix D) implying that the vortex becomes slightly elliptical.

From these asymptotic predictions, we have computed the Richardson number Ri_c at the vortex centre at the levels where the ambient shear is maximum. In Part 2, it will be shown that these two points are the locations where the Richardson number reaches its minimum or where the Kelvin–Helmholtz instability is first triggered. The results show that Ri_c cannot go below the value 3.43 in the limit $k_z F_h \to 0$. It therefore remains far from the critical value 1/4 necessary for the development of the shear instability. This result shows that the mechanism proposed by Lilly (1983), according to which the vertical shear should grow algebraically with time without bounds, is not valid when $k_z F_h$ is small for the flow studied herein. Because of the vertical coupling, neglected by Lilly (1983), the flow actually decays in the regions of high shear, thereby limiting the maximum vertical shear attainable. This is due to potential vorticity conservation and enhanced viscous effects. In addition, the squeezing of the isopycnals enhances the buoyancy vertical gradient in the regions of high shear.

These predictions will be compared to DNS in Part 2.

Acknowledgements

We thank D. Guy and V. Toai for technical assistance, and I. Delbende, F. Godeferd, S. Le Dizès, L. Oruba, R. Plougonven and the referees for helpful comments.

https://doi.org/10.1017/jfm.2020.226 Published online by Cambridge University Press

Declaration of interests

The authors report no conflict of interest.

Appendix A. Note on the scaling of the slow time

In this appendix, we discuss the particular choice for the scaling of the slow evolution. *A priori*, the most appropriate and classical choice for the slow time scale would be $\tilde{\tau} = \varepsilon t$ together with $\tilde{\tau} = O(1)$. Such scaling can be derived by equilibrating the magnitudes of the dominant terms of the final equation for the angular velocity obtained in § 4.1. However, the assumption $\tilde{\tau} = O(1)$ would violate the condition $\varepsilon U_S t < 1$, which ensures the validity of the long-wavelength assumption. To circumvent this difficulty, we consider in § 3 that the fast time is typically of order unity, $t = O(1)$, and that the slow evolution is such that $\partial/\partial t = \varepsilon^2 \partial/\partial \tau$ but without assuming $\tau = O(1)$. This scaling for $\partial/\partial t$ is required to balance the first-order forcing terms, which scale like $O(\varepsilon^2)$ when $t = O(1)$, so as to satisfy solvability conditions. It means that the time variations are weak of order ε^2 but the corresponding time is not large. However, it implies that the resulting equations over the slow time τ depend on the fast time t. At first sight, this could seem inconsistent, since fast and slow variables are generally assumed independent in multiscale expansions. However, this apparent paradox is removed subsequently since we do not use directly the equations involving t and τ but the rescaled equations expressed back solely in terms of the fast time t. An advantage of these assumptions is that they allow us to describe at leading order the initial transient dynamics for $t = O(1)$, which involves internal waves, as discussed in § 4.2.

Appendix B. Potentials

The potentials defined in (3.36) are given by

$$\Phi_s = \Phi_{ps} = \mathrm{M}(\Omega \mathscr{C}), \quad \Phi_{pc} = \mathrm{M}(\mathscr{C}\mathscr{F}), \quad \Phi_{p\Omega} = \mathrm{M}\left(\mathscr{C}\,(2+\mathscr{F})\,\frac{\partial \Omega}{\partial \tilde{z}}\right), \quad \text{(B 1}a\text{–}c\text{)}$$

$$\Phi_{wc} = -\frac{1}{2}\cos\left(\frac{t}{F_h}\right)\mathrm{M}(\mathscr{C}\mathscr{F}\cos(\Omega t)) - \sin\left(\frac{t}{F_h}\right)\mathrm{M}(\mathscr{C}\mathscr{G}\sin(\Omega t)), \quad \text{(B 2)}$$

$$\Phi_{ws} = -\frac{1}{2}\cos\left(\frac{t}{F_h}\right)\mathrm{M}(\mathscr{C}\mathscr{F}\sin(\Omega t)) + \sin\left(\frac{t}{F_h}\right)\mathrm{M}(\mathscr{C}\mathscr{G}\cos(\Omega t)), \quad \text{(B 3)}$$

where the operator M is defined as

$$\mathrm{M}(\chi(\tilde{r},\ldots)) = \tilde{r}\int_{+\infty}^{\tilde{r}} \chi(\xi,\ldots)\,\mathrm{d}\xi - \frac{1}{\tilde{r}}\int_0^{\tilde{r}} \xi^2 \chi(\xi,\ldots)\,\mathrm{d}\xi. \quad \text{(B 4)}$$

Appendix C. Streamfunctions

The streamfunctions defined in (3.38) are given by

$$\begin{aligned}\psi_{p\Omega} \;=\; & \tilde{r}\Omega\int_0^{\tilde{r}} \frac{1}{\eta^3\Omega^2}\int_0^{\eta} \xi^2\Omega(3+\mathscr{F})\mathscr{C}\frac{\partial \Omega}{\partial \tilde{z}}\,\mathrm{d}\xi\,\mathrm{d}\eta \\ & + \tilde{r}\Omega\int_{+\infty}^{\tilde{r}} (2+\mathscr{F})\frac{\mathscr{C}}{\Omega}\frac{\partial \Omega}{\partial \tilde{z}}\,\mathrm{d}\xi - \frac{\tilde{r}}{2}\frac{\partial \Phi_{p\Omega}}{\partial \tilde{r}}, \end{aligned} \quad \text{(C 1)}$$

https://doi.org/10.1017/jfm.2020.226 Published online by Cambridge University Press

$$\psi_{pc} = -\psi_s = -\tilde{r}\Omega \int_0^{\tilde{r}} \frac{1}{\eta^3\Omega^2} \int_0^{\eta} \xi^2\Omega^2\mathscr{C}\,\mathrm{d}\xi\,\mathrm{d}\eta - \tilde{r}\Omega \int_{+\infty}^{\tilde{r}} \mathscr{C}\,\mathrm{d}\xi + \frac{\tilde{r}}{2}\frac{\partial \Phi_{ps}}{\partial \tilde{r}}, \quad \text{(C 2)}$$

$$\begin{aligned}\psi_{ps} \;=\; & \frac{\tilde{r}}{2}\frac{\partial \Phi_{pc}}{\partial \tilde{r}} - \tilde{r}\int_{+\infty}^{\tilde{r}} \mathscr{C}\,\mathrm{d}\xi - 2F_h\tilde{r}\Omega \int_0^{\tilde{r}} \mathscr{C}\mathscr{G}\,\mathrm{d}\xi \\ & - 2F_h\tilde{r}\Omega \int_0^{\tilde{r}} \frac{1}{\eta^3\Omega^2} \int_0^{\eta} \xi^2\Omega^2\mathscr{C}\mathscr{G}\,\mathrm{d}\xi\,\mathrm{d}\eta \\ & + 2\tilde{r}\Omega \int_0^{\tilde{r}} \frac{1}{\eta^3\Omega^3} \int_0^{\eta} \xi^2\Omega^2\mathscr{C}\,\mathrm{d}\xi\,\mathrm{d}\eta - \tilde{r}\int_0^{\tilde{r}} \frac{1}{\eta^3\Omega^2} \int_0^{\eta} \xi^2\Omega^2\mathscr{C}\,\mathrm{d}\xi\,\mathrm{d}\eta. \quad \text{(C 3)}\end{aligned}$$

Appendix D. Determination of (Φ_{12}, ψ_{12})

Using the simplification (3.55) for the vertical velocity, equation (3.33) for the potential Φ_{12} reads

$$\begin{aligned}\nabla_h^2\Phi_{12} \;=\; & t\tilde{r}\Omega\frac{\partial\Omega}{\partial\tilde{r}}\left(\frac{\mathrm{d}U}{\mathrm{d}\tilde{z}}\right)^2\left[\cos(2\tilde{\theta}) - \frac{3}{2}\Omega t\sin(2\tilde{\theta})\right. \\ & \left. - \left(\cos(\Omega t - 2\tilde{\theta}) - \frac{t}{2}\Omega\,\sin(\Omega t - 2\tilde{\theta})\right)\cos\left(\frac{t}{F_h}\right)\right]. \quad \text{(D 1)}\end{aligned}$$

The solution, which is not singular at $\tilde{r} = 0$ and which vanishes at infinity, is

$$\begin{aligned}\Phi_{12} \;=\; & \frac{t}{2\tilde{r}^2}\left[\cos(2\tilde{\theta})\int_0^{\tilde{r}} \xi^3\Omega^2\,\mathrm{d}\xi - t\sin(2\tilde{\theta})\int_0^{\tilde{r}} \xi^3\Omega^3\,\mathrm{d}\xi\right. \\ & \left. - \cos\left(\frac{t}{F_h}\right)\int_0^{\tilde{r}} \xi^3\Omega^2\cos(\Omega t - 2\tilde{\theta})\,\mathrm{d}\xi\right]\left(\frac{\mathrm{d}U}{\mathrm{d}\tilde{z}}\right)^2. \quad \text{(D 2)}\end{aligned}$$

We can notice the presence of a term proportional to t^2 in the potential (D 2). Hence, the corresponding horizontal flow $\varepsilon^2\boldsymbol{\nabla}_h\Phi_{12}$ scales like ε^2t^2. This implies that the scaled first-order perturbation will be of order unity when $\varepsilon t = O(1)$, meaning that the expansion (3.4) is not uniformly asymptotic in time. This is the reason why the present results are *a priori* expected to be valid only when $\varepsilon t \ll 1$, as discussed in § 3.

Using (3.55) and (D 2), equation (3.34) for the streamfunction ψ_{12} is

$$\begin{aligned}\mathrm{L}(\psi_{12}) \;=\; & \left[\cos(2\tilde{\theta})\frac{\tilde{\tau}^2}{2\tilde{R}e_b}\tilde{r}\frac{\partial}{\partial\tilde{r}}\left(\frac{1}{\tilde{r}}\frac{\partial\zeta_0}{\partial\tilde{r}}\right) + t\cos(2\tilde{\theta})\left(\frac{\tilde{r}}{3}\frac{\partial\Omega^3}{\partial\tilde{r}} + \frac{1}{\tilde{r}^3}\frac{\partial\zeta_0}{\partial\tilde{r}}\int_0^{\tilde{r}} \xi^3\Omega^2\,\mathrm{d}\xi\right)\right. \\ & \left. + \sin(2\tilde{\theta})\left(\frac{\tilde{r}}{2}\frac{\partial\Omega^2}{\partial\tilde{r}} + t^2\frac{\tilde{r}}{4}\frac{\partial\Omega^4}{\partial\tilde{r}} - \frac{t^2}{\tilde{r}^3}\frac{\partial\zeta_0}{\partial\tilde{r}}\int_0^{\tilde{r}} \xi^3\Omega^3\,\mathrm{d}\xi\right) + \mathscr{F}_w\right]\left(\frac{\mathrm{d}U}{\mathrm{d}\tilde{z}}\right)^2, \\ & \quad \text{(D 3)}\end{aligned}$$

https://doi.org/10.1017/jfm.2020.226 Published online by Cambridge University Press

where $\mathscr{F}_w$ gathers the terms due to internal waves,

$$\mathscr{F}_w = -\left[\frac{t}{\tilde{r}^3}\frac{\partial\zeta_0}{\partial\tilde{r}}\int_0^{\tilde{r}}\xi^3\Omega^2\cos(\Omega t-2\tilde{\theta})\,\mathrm{d}\xi-\frac{\tilde{r}}{3}\frac{\partial\Omega^3}{\partial\tilde{r}}t\cos(\Omega t-2\tilde{\theta})\right.$$
$$\left.-\frac{\tilde{r}}{2}\frac{\partial\Omega^2}{\partial\tilde{r}}\left(1-\frac{t^2}{2}\Omega^2\right)\sin(\Omega t-2\tilde{\theta})\right]\cos\left(\frac{t}{F_h}\right), \tag{D 4}$$

and we remind the reader that $\tilde{\tau}=\varepsilon t$. The solution is sought in the form

$$\psi_{12}=\frac{1}{2}\left[-\cos(2\tilde{\theta})\psi_{2b}+\sin(2\tilde{\theta})\left(t\psi_{2s}+\frac{\tilde{\tau}^2\psi^v_{2s}}{\tilde{Re}_b}\right)-t^2\cos(2\tilde{\theta})\psi_{2c}+\psi^w_{12}\right]\left(\frac{\mathrm{d}U}{\mathrm{d}\tilde{z}}\right)^2, \tag{D 5}$$

where the streamfunctions ψ_{2b}, ψ_{2s}, ψ_{2c}, ψ^v_{2s} and ψ^w_{12} are solutions of

$$\frac{\nabla^{2*}_{\tilde{r}}\psi_{2s}}{2}+\Omega\nabla^{2*}_{\tilde{r}}\psi_{2b}-\frac{1}{\tilde{r}}\frac{\partial\zeta_0}{\partial\tilde{r}}\psi_{2b}=\tilde{r}\Omega\frac{\partial\Omega}{\partial\tilde{r}}, \tag{D 6}$$

$$-\nabla^{2*}_{\tilde{r}}\psi_{2c}+\Omega\nabla^{2*}_{\tilde{r}}\psi_{2s}-\frac{1}{\tilde{r}}\frac{\partial\zeta_0}{\partial\tilde{r}}\psi_{2s}=\tilde{r}\Omega^2\frac{\partial\Omega}{\partial\tilde{r}}+\frac{1}{\tilde{r}^3}\frac{\partial\zeta_0}{\partial\tilde{r}}\int_0^{\tilde{r}}\xi^3\Omega^2\,\mathrm{d}\xi, \tag{D 7}$$

$$\Omega\nabla^{2*}_{\tilde{r}}\psi_{2c}-\frac{1}{\tilde{r}}\frac{\partial\zeta_0}{\partial\tilde{r}}\psi_{2c}=\tilde{r}\Omega^3\frac{\partial\Omega}{\partial\tilde{r}}-\frac{1}{\tilde{r}^3}\frac{\partial\zeta_0}{\partial\tilde{r}}\int_0^{\tilde{r}}\xi^3\Omega^3\,\mathrm{d}\xi, \tag{D 8}$$

$$\Omega\nabla^{2*}_{\tilde{r}}\psi^v_{2s}-\frac{1}{\tilde{r}}\frac{\partial\zeta_0}{\partial\tilde{r}}\psi^v_{2s}=\frac{1}{2}\left[\frac{\partial^2\zeta_0}{\partial\tilde{r}^2}-\frac{1}{\tilde{r}}\frac{\partial\zeta_0}{\partial\tilde{r}}\right], \tag{D 9}$$

$$\mathrm{L}(\psi^w_{12})=2\mathscr{F}_w, \tag{D 10}$$

where $\nabla^{2*}_{\tilde{r}}$ is defined as

$$\nabla^{2*}_{\tilde{r}}\varphi=\frac{\partial^2\varphi}{\partial\tilde{r}^2}+\frac{1}{\tilde{r}}\frac{\partial\varphi}{\partial\tilde{r}}-\frac{4\varphi}{\tilde{r}^2}. \tag{D 11}$$

Like for the potential Φ_{12}, the streamfunction (D 5) contains a term scaling like t^2, which implies that the scaled first-order perturbation is of order ε^2t^2, i.e. of order unity when $\tilde{\tau}=\varepsilon t=O(1)$, making the expansion (3.4) not uniformly asymptotic in time.

In (D 6)–(D 9), the angular velocity Ω and vertical vorticity ζ_0 evolve on the slow time according to (3.62). In § 4.1, it is shown that this evolution can be very well accounted for by assuming that the vortex keeps a Lamb–Oseen profile but with time-varying maximum angular velocity $\Omega_c(\tilde{z},\tau)$ and radius $\tilde{a}_e(\tilde{z},\tau)$:

$$\Omega=\Omega_c(\tilde{z},\tau)\bar{\Omega}(\bar{r}),\quad \bar{\Omega}=\frac{1-\exp(-\bar{r}^2)}{\bar{r}^2}, \tag{D 12a,b}$$

where $\bar{r}=\tilde{r}/\tilde{a}_e$. Then, by writing ψ_{2b}, ψ_{2s}, ψ_{2c} and ψ^w_{12} as

$$\psi_{2b}=\tilde{a}_e^2\Omega_c\bar{\psi}_{2b}(\bar{r}),\quad \psi_{2s}=\tilde{a}_e^2\Omega_c^2\bar{\psi}_{2s}(\bar{r}),\quad \psi_{2c}=\tilde{a}_e^2\Omega_c^3\bar{\psi}_{2c}(\bar{r}),\quad \psi^v_{2s}=\bar{\psi}^v_{2s}(\bar{r}), \tag{D 13a–d}$$

the equations for $\bar{\psi}_{2b}$, $\bar{\psi}_{2s}$, $\bar{\psi}_{2c}$ and $\bar{\psi}^v_{2s}$ remain identical to (D 6)–(D 9) except for the changes $\tilde{r}\to\bar{r}$, $\Omega\to\bar{\Omega}$ and $\zeta_0\to\bar{\zeta}_0$. This implies that they depend only on $\bar{r}$ and no longer on $(\tilde{z},\tau)$, meaning that they can be solved once and for all. These four equations share the same linear operator, which admits a homogeneous solution

https://doi.org/10.1017/jfm.2020.226 Published online by Cambridge University Press

behaving as $\bar{\psi}_{2h} = \bar{r}^2$ for $\bar{r} \to +\infty$ and as $\bar{\psi}_{2h} = 2.524\bar{r}^2$ for $\bar{r} \to 0$ (Moore & Saffman 1975; Le Dizès & Laporte 2002). By using this homogeneous solution, it is possible to determine numerically the complete solutions that vanish at infinity and are non-singular at $\bar{r} = 0$. As shown in figure 2(*c*), they all rapidly vanish outside the vortex core. For $\bar{r} \ll 1$, they behave as

$$\bar{\psi}_{2b} = \beta_2 \bar{r}^2, \quad \bar{\psi}_{2s} = \sigma_2 \bar{r}^2, \quad \bar{\psi}_{2c} = \chi_2 \bar{r}^2, \quad \bar{\psi}^v_{2s} = \sigma^v_2 \bar{r}^2, \tag{D 14a–d}$$

where the neglected terms are $O(\bar{r}^4)$ and the coefficients are

$$\beta_2 = -0.1506, \quad \sigma_2 = 0.3786, \quad \chi_2 = -9.830 \times 10^{-3}, \quad \sigma^v_2 = -1.524. \tag{D 15a–d}$$

Finally, ψ^w_{12} can be computed numerically from (D 10) following a similar approach as implemented to determine ψ_{wc} and ψ_{ws} in § 3.2.1. The initial condition is $\psi^w_{12} = \psi_{2b}\cos(2\tilde{\theta})$ such that the total streamfunction (D 5) vanishes at $t = 0$. The evolution of Ω can be taken into account by directly integrating (4.2) numerically. For $\tilde{r} \ll 1$, ψ^w_{12} is also of the form

$$\psi^w_{12} = \tilde{r}^2[f_c(t, \tilde{z}, \tau)\cos(2\theta) + f_s(t, \tilde{z}, \tau)\sin(2\theta)]\left(\frac{\mathrm{d}U}{\mathrm{d}\tilde{z}}\right)^2. \tag{D 16}$$

By using (D 13), this implies that the streamfunction ψ_{12} behaves in the vicinity of the vortex core as

$$\begin{aligned}\psi_{12} = \frac{\tilde{r}^2}{2}\Bigg[&\left(\sigma_2\Omega_c^2 t + \frac{\sigma^v_2\Omega_c\tilde{\tau}^2}{\tilde{Re}_b} + f_s\right)\sin(2\tilde{\theta}) \\ &- (\beta_2\Omega_c + \chi_2\Omega_c^3 t^2 - f_c)\cos(2\tilde{\theta})\Bigg]\left(\frac{\mathrm{d}U}{\mathrm{d}\tilde{z}}\right)^2.\end{aligned} \tag{D 17}$$

In § 4.3, this allows us to determine the evolution of the vertical shear of the horizontal velocity and the Richardson number on the vortex axis. We have also computed the streamfunctions ψ_{2b}, ψ_{2s} and ψ_{2c} directly from (D 6)–(D 8) without using the empirical profile (D 12) but by using the angular velocity obtained from the numerical integration of (3.62). They turn out to be very close to those plotted in figure 2(*c*) confirming the validity of the assumption (D 12).

Appendix E. Derivation of the streamfunction ψ_w for small time

In this appendix, we derive analytically the streamfunctions ψ_{wc} and ψ_{ws} associated to internal waves for small time. This will allow us to obtain the asymptotic expressions of $\mathscr{C}_w$ and $\mathscr{S}_w$ for $t \ll 1$.

For $t \ll 1$, the right-hand sides of (3.44) and (3.45) can be expanded in powers of t, giving

$$\frac{\partial\nabla^2_{\tilde{r}}\psi_{wc}}{\partial t} + \Omega\nabla^2_{\tilde{r}}\psi_{ws} - \frac{1}{\tilde{r}}\frac{\partial\zeta_0}{\partial\tilde{r}}\psi_{ws} = f_0 + t^2\frac{f_2}{2F_h^2} + O(t^4), \tag{E 1}$$

$$\frac{\partial\nabla^2_{\tilde{r}}\psi_{ws}}{\partial t} - \Omega\nabla^2_{\tilde{r}}\psi_{wc} + \frac{1}{\tilde{r}}\frac{\partial\zeta_0}{\partial\tilde{r}}\psi_{wc} = tf_1 + t^3\frac{f_3}{6F_h^2} + O(t^4), \tag{E 2}$$

https://doi.org/10.1017/jfm.2020.226 Published online by Cambridge University Press

where $f_0 = -\mathrm{K}(\mathscr{C}\mathscr{F})$, $f_1 = \mathrm{K}(\mathscr{C}\Omega)$, $f_2 = \mathrm{K}(\tilde{r}\Omega^2)$ and $f_3 = \mathrm{K}(\tilde{r}\Omega^3)$, where the operator K is defined as

$$\mathrm{K}(\chi(\tilde{r},\ldots)) = \zeta_0\chi(\tilde{r},\ldots) + \frac{1}{2}\frac{\partial\zeta_0}{\partial\tilde{r}}\left[\int_{+\infty}^{\tilde{r}}\chi(\xi,\ldots)\,\mathrm{d}\xi + \frac{1}{\tilde{r}^2}\int_0^{\tilde{r}}\xi^2\chi(\xi,\ldots)\,\mathrm{d}\xi\right]. \quad (\mathrm{E}\,3)$$

Accordingly, the solutions of (E 1) and (E 2) are expressed as

$$\psi_{wc} = t\psi_{w1} + t^3\frac{\psi_{w3}}{F_h^2} + O(t^5), \quad \psi_{ws} = \psi_{w0} + t^2\psi_{w2} + t^4\frac{\psi_{w4}}{F_h^2} + O(t^5). \quad (\mathrm{E}\,4a,b)$$

Inserting this expansion in (E 1) and (E 2) yields the sequence of equations

$$\nabla_{\tilde{r}}^2\psi_{w1} + \Omega\nabla_{\tilde{r}}^2\psi_{w0} - \frac{1}{\tilde{r}}\frac{\partial\zeta_0}{\partial\tilde{r}}\psi_{w0} = -f_0, \quad (\mathrm{E}\,5)$$

$$2\nabla_{\tilde{r}}^2\psi_{w2} - \Omega\nabla_{\tilde{r}}^2\psi_{w1} + \frac{1}{\tilde{r}}\frac{\partial\zeta_0}{\partial\tilde{r}}\psi_{w1} = -f_1, \quad (\mathrm{E}\,6)$$

$$3\nabla_{\tilde{r}}^2\psi_{w3} + F_h^2\left(\Omega\nabla_{\tilde{r}}^2\psi_{w2} - \frac{1}{\tilde{r}}\frac{\partial\zeta_0}{\partial\tilde{r}}\psi_{w2}\right) = -\frac{f_2}{2}, \quad (\mathrm{E}\,7)$$

$$4\nabla_{\tilde{r}}^2\psi_{w4} - \Omega\nabla_{\tilde{r}}^2\psi_{w3} + \frac{1}{\tilde{r}}\frac{\partial\zeta_0}{\partial\tilde{r}}\psi_{w3} = -\frac{f_3}{6}, \quad (\mathrm{E}\,8)$$

where the operator $\nabla_{\tilde{r}}^2$ is defined in (3.43). Since $t \ll 1$, the angular velocity Ω in (E 5)–(E 8) can be assumed equal to its initial profile (2.11).

These equations can be solved successively. We first impose

$$\psi_{w0} = -[\psi_{ps} + \lambda_0\tilde{r}\Omega + (\lambda_1 - \vartheta)\tilde{r}], \quad (\mathrm{E}\,9)$$

where ψ_{ps} is defined in (C 3), in order to satisfy the same initial condition (3.46) as for the solution computed numerically. Then, (E 5) gives $\psi_{w1} = -\psi_{pc} - (\lambda_1 - \vartheta)\tilde{r}\Omega - \mathscr{A}\tilde{r}/2$, where ψ_{pc} is defined in (C 2) and where it has also been imposed that $\psi_{w1} \to 0$ as $\tilde{r} \to +\infty$. In turn, (E 6) yields $\psi_{w2} = \mathscr{A}\tilde{r}\Omega/4$, while (E 7) gives

$$\begin{aligned}\psi_{w3} = -\frac{1}{12}\Bigg[&\tilde{r}\Omega\int_{+\infty}^{\tilde{r}}\xi\Omega^2\,\mathrm{d}\xi + \frac{\Omega}{\tilde{r}}\int_0^{\tilde{r}}\xi^3\Omega^2\,\mathrm{d}\xi - \tilde{r}\int_{+\infty}^{\tilde{r}}\xi\Omega^3\,\mathrm{d}\xi - \frac{1}{\tilde{r}}\int_0^{\tilde{r}}\xi^3\Omega^3\,\mathrm{d}\xi \\ &+ 4\tilde{r}\int_{+\infty}^{\tilde{r}}\frac{\Omega}{\eta^3}\int_0^{\eta}\xi^3\Omega^2\,\mathrm{d}\xi\Bigg], \end{aligned} \quad (\mathrm{E}\,10)$$

where the constants of integration have been chosen so that ψ_{w3} vanishes at infinity. At fourth order, only $\nabla_{\tilde{r}}^2\psi_{w4}$ will be needed: it is not necessary to derive ψ_{w4}. From (E 8), we have directly that

$$\nabla_{\tilde{r}}^2\psi_{w4} = -\frac{1}{24}\left(\frac{6}{\tilde{r}}\frac{\partial\zeta_0}{\partial\tilde{r}}\psi_{w3} + \Omega f_2 + f_3\right). \quad (\mathrm{E}\,11)$$

Finally, we impose that the mean displacement associated with the internal waves is zero, giving from (3.48)

$$\mathscr{C}_w(t) = -\vartheta t + \frac{\varsigma}{F_h^2}t^3 + O(t^5), \quad \mathscr{S}_w(t) = -\frac{\mathscr{A}}{4}t^2 + \frac{\sigma}{F_h^2}t^4 + O(t^5), \quad (\mathrm{E}\,12a,b)$$

https://doi.org/10.1017/jfm.2020.226 Published online by Cambridge University Press

where (3.42) has been used and where

$$\varsigma = -\tfrac{1}{12}\langle f_2, \tilde{r}\rangle = -3.554\times 10^{-2}, \quad \sigma = \tfrac{1}{2}\langle \nabla_{\tilde{r}}^2 \psi_{w4}, \tilde{r}\rangle = -3.826\times 10^{-3}, \qquad (\mathrm{E}\,13a,b)$$

for the Lamb–Oseen profile.

Appendix F. Asymptotic analysis of equation (4.6)

In this appendix, we solve equation (4.6) for the angular velocity when $\gamma \ll 1$ and $\gamma \gg 1$ by matched asymptotic analyses.

F.1. *Small* γ

When $\gamma \ll 1$, the solution of (4.6) can be expanded as

$$\Omega = \Omega_0 + \gamma\,\Omega_1 + O(\gamma^2), \qquad (\mathrm{F}\,1)$$

and we introduce a slow time scale $\upsilon = \gamma\tilde{t}$. At leading order when $\tilde{t}^{1/3} \ll 1/\gamma$, i.e. in terms of the original parameters $t \ll ReF_h^2$, (4.6) becomes

$$\frac{\partial \Omega_0}{\partial \tilde{t}} = -\frac{\Omega_0^3}{3\tilde{t}^{1/3}}, \qquad (\mathrm{F}\,2)$$

whose solution is

$$\Omega_0 = \frac{\Omega_i(\tilde{r},\upsilon)}{\sqrt{1+\tilde{t}^{2/3}\Omega_i^2(\tilde{r},\upsilon)}}, \qquad (\mathrm{F}\,3)$$

where Ω_i is the angular velocity profile at $\tilde{t}=0$. It can depend also on the slow time υ. At next order, we obtain

$$\frac{\partial \Omega_1}{\partial \tilde{t}} + \frac{\partial \Omega_0}{\partial \upsilon} = -\frac{\Omega_0^2\Omega_1}{\tilde{t}^{1/3}} + \frac{1}{6\tilde{r}}\frac{\partial \zeta_0}{\partial \tilde{r}}. \qquad (\mathrm{F}\,4)$$

After substituting (F 3) in this equation, its general solution is found to be

$$\Omega_1 = \frac{\Theta - \dfrac{\partial \Omega_i}{\partial \upsilon} + \dfrac{1}{6\tilde{r}}\dfrac{\partial \zeta_i}{\partial \tilde{r}} - \dfrac{1}{2}\left(\dfrac{\partial \Omega_i}{\partial \tilde{r}}\right)^2\left[\dfrac{3\arctan(\Omega_i\tilde{t}^{1/3})}{\Omega_i^4} - \dfrac{3\tilde{t}^{1/3}}{\Omega_i^3} + \dfrac{\tilde{t}}{\Omega_i}\right]}{(1+\tilde{t}^{2/3}\Omega_i^2)^{3/2}}, \qquad (\mathrm{F}\,5)$$

where Θ is an arbitrary constant. This constant should be set to zero to ensure that $\Omega_1 \to 0$ as $\tilde{r} \to +\infty$. In addition, we have to impose that $\Omega = \Omega_i$ initially, implying that $\Omega_1 = 0$ at $\tilde{t} = 0$. This leads to an equation for Ω_i over the slow time υ:

$$\frac{\partial \Omega_i}{\partial \upsilon} = \frac{1}{6\tilde{r}}\frac{\partial \zeta_i}{\partial \tilde{r}}. \qquad (\mathrm{F}\,6)$$

Since $\Omega_i(\tilde{r}, \upsilon = 0) = [1 - \exp(-\tilde{r}^2)]/\tilde{r}^2$, the solution of (F 6) is

$$\Omega_i = \frac{1-\exp(-\tilde{r}^2/\tilde{a}^2)}{\tilde{r}^2}, \qquad (\mathrm{F}\,7)$$

https://doi.org/10.1017/jfm.2020.226 Published online by Cambridge University Press

with $\tilde{a}^2 = 1 + 2\upsilon/3$. Gathering the two orders and rescaling the slow time scale υ gives the expression (4.7) of Ω.

F.2. *Large* γ

When $\gamma \gg 1$, the second term on the right-hand side of (4.6) is dominant provided that $\gamma \gg 1/\tilde{t}^{1/3}$, i.e. when the original time is such that $t \gg ReF_h^2$. In this time range, (4.6) reduces at leading order to

$$\frac{\partial \Omega}{\partial \tilde{t}} = \frac{\gamma}{6\tilde{r}} \frac{\partial \zeta_0}{\partial \tilde{r}}. \tag{F 8}$$

The solution is

$$\Omega = \frac{1 - \exp(-\tilde{r}^2/\tilde{a}^2)}{\tilde{r}^2}, \tag{F 9}$$

with $\tilde{a}^2 = a_0^2 + 2\gamma\tilde{t}/3$, where a_0 is an arbitrary constant.

The solution (F 9) is not valid for small time $\tilde{t} \lesssim 1/\gamma^3$. In order to find a solution for small time, we rescale the time $\tilde{t} = \alpha\upsilon$ with $0 < \alpha < O(1/\gamma^3)$ and $\upsilon = O(1)$. Then, (4.6) becomes

$$\frac{\partial \Omega}{\partial \upsilon} = -\alpha^{2/3} \frac{\Omega^3}{3\upsilon^{1/3}} + \frac{\alpha\gamma}{6\tilde{r}} \frac{\partial \zeta_0}{\partial \tilde{r}}. \tag{F 10}$$

This equation shows that $\partial\Omega/\partial\upsilon \simeq 0$ at leading order since the magnitudes of $\alpha^{2/3}$ and $\alpha\gamma$ are at most $O(1/\gamma^2)$. In other words, the angular velocity remains equal to its initial profile

$$\Omega = \frac{1 - \exp(-\tilde{r}^2)}{\tilde{r}^2}, \tag{F 11}$$

as long as $\alpha\gamma \ll 1$, i.e $\tilde{t} \ll 1/\gamma$.

In the overlap interval $1/\gamma^3 \ll \tilde{t} \ll 1/\gamma$, the two solutions (F 9) and (F 11) are both valid and thus should match. This imposes $a_0 = 1$. Therefore, an approximation of the solution of (4.6) valid for all time for $\gamma \gg 1$ is (F 9) with $\tilde{a}^2 = 1 + 2\gamma\tilde{t}/3$. This implies that the angular velocity at the vortex centre evolves as $\Omega_c = 1/(1 + 2\gamma\tilde{t}/3)$. Since $\tilde{t}^{1/3} \ll 1 + 2\gamma\tilde{t}/3$ whatever $\tilde{t}$ when $\gamma \gg 1$, this approximation is in fact approximately equal to the one for $\gamma \ll 1$ (see 4.9). Thus, equations (4.9) and (4.10) can be used not only for $\gamma \ll 1$ but also for $\gamma \gg 1$.

REFERENCES

AUGIER, P. & BILLANT, P. 2011 Onset of secondary instabilities on the zigzag instability in stratified fluids. *J. Fluid Mech.* **682**, 120–131.

AUGIER, P., CHOMAZ, J.-M. & BILLANT, P. 2012 Spectral analysis of the transition to turbulence from a dipole in stratified fluid. *J. Fluid Mech.* **713**, 86–108.

BILLANT, P. 2010 Zigzag instability of vortex pairs in stratified and rotating fluids. Part 1. General stability equations. *J. Fluid Mech.* **660**, 354–395.

BILLANT, P. & BONNICI, J. 2020 Evolution of a vortex in a strongly stratified shear flow. Part 2. Numerical simulations. *J. Fluid Mech.* **893**, A18.

BILLANT, P. & CHOMAZ, J.-M. 2000 Three-dimensional stability of a vertical columnar vortex pair in a stratified fluid. *J. Fluid Mech.* **419**, 65–91.

BILLANT, P. & CHOMAZ, J.-M. 2001 Self-similarity of strongly stratified inviscid flows. *Phys. Fluids* **13**, 1645–1651.

https://doi.org/10.1017/jfm.2020.226 Published online by Cambridge University Press

BONNICI, J. 2018 Décorrélation verticale d'un tourbillon soumis à un champ de cisaillement dans un fluide fortement stratifié. PhD thesis, LadHyX, Université Paris-Saclay.

BOULANGER, N., MEUNIER, P. & LE DIZÈS, S. 2007 Structure of a stratified tilted vortex. *J. Fluid Mech.* **583**, 443–458.

BOULANGER, N., MEUNIER, P. & LE DIZÈS, S. 2008 Tilt-induced instability of a stratified vortex. *J. Fluid Mech.* **596**, 1–20.

BRETHOUWER, G., BILLANT, P., LINDBORG, E. & CHOMAZ, J.-M. 2007 Scaling analysis and simulation of strongly stratified turbulent flows. *J. Fluid Mech.* **585**, 343–368.

DELONCLE, A., BILLANT, P. & CHOMAZ, J.-M. 2008 Nonlinear evolution of the zigzag instability in stratified fluids: a shortcut on the route to dissipation. *J. Fluid Mech.* **599**, 229–239.

DEMARIA, M. 1996 The effect of vertical shear on tropical cyclone intensity change. *J. Atmos. Sci.* **53**, 2076–2088.

FRANK, W. M. & RITCHIE, E. A. 1999 Effects of environmental flow upon tropical cyclone structure. *Mon. Weath. Rev.* **127**, 2044–2061.

GODEFERD, F. S. & STAQUET, C. 2003 Statistical modelling and direct numerical simulations of decaying stably stratified turbulence. Part 2. Large-scale and small-scale anisotropy. *J. Fluid Mech.* **486**, 115–159.

HERRING, J. R. & MÉTAIS, O. 1989 Numerical experiments in forced stably stratified turbulence. *J. Fluid Mech.* **202**, 97–115.

HOWARD, L. N. 1961 Note on a paper of John W. Miles. *J. Fluid Mech.* **10**, 509–512.

JONES, S. C. 1995 The evolution of vortices in vertical shear. I. Initially barotropic vortices. *Q. J. R. Meteorol. Soc.* **121**, 821–851.

JONES, S. C. 2000*a* The evolution of vortices in vertical shear. II. Large-scale asymmetries. *Q. J. R. Meteorol. Soc.* **126**, 3137–3159.

JONES, S. C. 2000*b* The evolution of vortices in vertical shear. III. Baroclinic vortices. *Q. J. R. Meteorol. Soc.* **126**, 3161–3185.

JONES, S. C. 2004 On the ability of dry tropical-cyclone-like vortices to withstand vertical shear. *J. Atmos. Sci.* **61**, 114–119.

LAVAL, J.-P., MCWILLIAMS, J. C. & DUBRULLE, B. 2003 Forced stratified turbulence: successive transitions with Reynolds number. *Phys. Rev.* E **68** (3), 036308.

LE DIZÈS, S. & LAPORTE, F. 2002 Theoretical predictions for the elliptical instability in a two-vortex flow. *J. Fluid Mech.* **471**, 169–201.

LILLY, D. K. 1983 Stratified turbulence and the mesoscale variability of the atmosphere. *J. Atmos. Sci.* **40**, 749–761.

LINDBORG, E. 2006 The energy cascade in a strongly stratified fluid. *J. Fluid Mech.* **550**, 207–242.

MAJDA, A. J. & GROTE, M. J. 1997 Model dynamics and vertical collapse in decaying strongly stratified flows. *Phys. Fluids* **9**, 2932–2940.

MARSHALL, J. S. & PARTHASARATHY, B. 1993 Tearing of an aligned vortex by a current difference in two-layer quasi-geostrophic flow. *J. Fluid Mech.* **255**, 157–182.

MILES, J. W. 1961 On the stability of heterogeneous shear flows. *J. Fluid Mech.* **10**, 496–508.

MOORE, D. W. & SAFFMAN, P. G. 1975 The instability of a straight vortex filament in a strain field. *Proc. R. Soc. Lond.* A **346** (1646), 413–425.

PÄSCHKE, E., MARSCHALIK, P., OWINOH, A. Z. & KLEIN, R. 2012 Motion and structure of atmospheric mesoscale baroclinic vortices: dry air and weak environmental shear. *J. Fluid Mech.* **701**, 137–170.

REASOR, P. D., MONTGOMERY, M. T. & GRASSO, L. D. 2004 A new look at the problem of tropical cyclones in vertical shear flow: vortex resiliency. *J. Atmos. Sci.* **61**, 3–22.

RILEY, J. J. & DEBRUYNKOPS, S. M. 2003 Dynamics of turbulence strongly influenced by buoyancy. *Phys. Fluids* **15**, 2047–2059.

RILEY, J. J. & LELONG, M.-P. 2000 Fluid motions in the presence of strong stable stratification. *Annu. Rev. Fluid Mech.* **32**, 613–657.

SMITH, R. K., ULRICH, W. & SNEDDON, G. 2000 On the dynamics of hurricane-like vortices in vertical-shear flows. *Q. J. R. Meteorol. Soc.* **126**, 2653–2670.

https://doi.org/10.1017/jfm.2020.226 Published online by Cambridge University Press

SUTYRIN, G. G. & MOREL, Y. G. 1997 Intense vortex motion in a stratified fluid on the beta-plane: an analytical theory and its validation. *J. Fluid Mech.* **336**, 203–220.

VANDERMEIRSCH, F., MOREL, Y. & SUTYRIN, G. 2001 The net advective effect of a vertically sheared current on a coherent vortex. *J. Phys. Oceanogr.* **31**, 2210–2225.

VANDERMEIRSCH, F., MOREL, Y. & SUTYRIN, G. 2002 Resistance of a coherent vortex to a vertical shear. *J. Phys. Oceanogr.* **32**, 3089–3100.

WAITE, M. L. 2013 The vortex instability pathway in stratified turbulence. *J. Fluid Mech.* **716**, 1–4.

WAITE, M. L. & BARTELLO, P. 2004 Stratified turbulence dominated by vortical motion. *J. Fluid Mech.* **517**, 281–308.

https://doi.org/10.1017/jfm.2020.226 Published online by Cambridge University Press